Ling et al. *Microsystems & Nanoengineering* (2026)12:61
https://doi.org/10.1038/s41378-025-01142-8

Microsystems & Nanoengineering
www.nature.com/micronano

REVIEW ARTICLE Open Access

Toward continuous monitoring systems: emerging trends of on-chip sensors in organ-on-a-chip

Shuang Ling[1], Chenrui Xu[2], Yuqing Jiang[1], Feng Xu[1], Hang Jin[1], Hong Chen[1], Songyue Chen[1]✉, Zhengmao Ding[1]✉ and Daoheng Sun[1]✉

Abstract

The emergence of Organ-on-a-Chip (OoC) has significantly advanced biomedical research mainly on aspects of disease modeling and drug research. The need for real-time and continuous monitoring of the OoCs has been driving the development of integrated sensors on-chip. To meet these needs across different scales, from microscopic to macroscopic, primary sensing strategies for in situ sensor integration typically include electrical, optical, and mechanical approaches. This review focuses on the detection methodologies driven by these requirements and analyzes the core sensing elements involved. It further explores current innovative pathways for achieving in situ sensing integration and discusses the future prospects brought about by the development of models in OoC and sensing technologies.

Introduction

Organ-on-a-Chip (OoC) is an emerging technology that constructs three-dimensional tissue microstructures on an in vitro chip to simulate human organ functions[1]. Its emergence represents a transformative advancement in biomedical research, with profound significance for multiple domains, spanning basic life science, preclinical drug development, and personalized medicine[2].

The development of OoC technology dates back to 1997. Hosokawa et al. fabricated a microbial bioreactor using conventional MEMS fabrication techniques, taking the inaugural step toward realizing the concepts of "cell-on-a-chip"[3,4]. In 2010, the Ingber's team at Harvard University pioneered the "lung-on-a-chip"[5], marking the official birth of OoC technology. OoC platforms recapitulate key structural, functional and physiological features of human organs through microengineered systems, address critical limitations of traditional in vitro models and animal studies[6,7]. Current OoC models include "heart-on-a-chip", "liver-on-a-chip", "brain-on-a-chip", "intestine-on-a-chip", either single-organ models or multi-organ models[8–10].

Despite groundbreaking progress in biomimetic OoC systems, a there is a growing need for dynamic and in situ monitoring of tissue/organ functions and microenvironments on-chip in order to promote large-scale and automation applications. Traditional detection methods are mainly endpoint offline tests (such as enzyme linked immunosorbent assay; ELISA, mass spectrometry, etc.), which require tedious manual sample collection and is less applicable for integration with OoC platforms[11–13]. The emerging on-chip in situ sensing technologies (including electrical, optical, mechanical, etc) achieved continuous monitoring of cell behavior[14,15], metabolic products[16,17], and environmental parameters[18,19], providing a promising solution for the functional integration of OoC. Ferrell developed a dual-layer microfluidic system in 2010, integrating transepithelial electrical resistance (TEER) measurement electrodes to assess renal epithelial cells. The device enabled monitoring of cell growth and tight junction integrity under physiologically relevant flow conditions[20]. This represents an early instance of sensor integration in OoC systems. In 2016, Lewis' team at Harvard University pioneered the first fully 3D-printed OoC with integrated sensors[21]. By 2017, Ali et al. achieved

Correspondence: Songyue Chen (s.chen@xmu.edu.cn) or Zhengmao Ding (dzm@xmu.edu.cn) or Daoheng Sun (sundh@xmu.edu.cn)
[1]Pen-Tung Sah Institute of Micro-Nano Science and Technology, Xiamen University, Xiamen, China
[2]School of Electronic Science and Engineering (National Model Microelectronics College), Xiamen University, Xiamen, China
These authors contributed equally: Shuang Ling, Chenrui Xu

in situ, continuous, and automated monitoring of biophysical and biochemical parameters within the microenvironment via a fully integrated modular platform encompassing physical, chemical, and optical sensing[22]. These advancements provide robust new tools for in situ sensing in OoC systems, signifying a pivotal evolution toward more precise, real-time, and efficient OoC technology.

This review focuses on in situ sensing technologies within OoC systems, and systematically summarized the features and applications of various existing sensing technologies on OoC based on the specific sensing needs of different organs. On this basis, it elaborates on the performance and classification of the core sensing elements, explored the latest development trends, as well as the rising challenges, aiming to provide ideas and insights toward achieving multi-functional and integrated on-chip sensing capabilities in OoC platforms.

Sensing needs driven by application scenarios

As the detection source for on-chip sensors, the construction of in vitro tissue models is a necessary first step. Table 1 summarized the tissue models of various organs that have been established in vitro, based on the core application scenarios of OoC.

As shown in the table, OoC systems are primarily applied in disease modeling and drug analysis, with the latter focusing on evaluating compound toxicity and monitoring. metabolic function. Key organ models here include the heart, liver, kidney, and nervous system.

Due to the specialty of different organs, the specific monitoring requirements are quite different. As an electromechanically coupled organ, the heart's functionality is characterized through its rhythmic electrical excitation and subsequent physical contraction. Drug-induced cardiotoxicity often manifests as arrhythmias (electrical abnormality) and contractile dysfunction (mechanical abnormality). Therefore, besides biomarkers, electrical and mechanical sensors are employed to quantify the contraction[23–30]. The liver and kidney play a crucial role in metabolism, necessitating the monitoring of specific secreted biomarkers, which are generally converted to quantifiable electrical signals[31]. Neural function is intrinsically electrical, relying on the coordinated firing of action potentials across networks of neurons. Such sensing scenarios require to capture the spatiotemporal patterns of network-wide firing, which places high demands on the spatiotemporal resolution of the sensors[32]. The distinction between disease analysis models and drug analysis models primarily lies in their construction methods, while the target analytes they detect are often similar. In liver injury models, the monitoring of target molecules (GST-α; TGF-β) similarly relies on optical and electrochemical biosensors. These two types of biosensors are key technologies for achieving real-time and highly sensitive monitoring[33,34].

Most current models require additional endpoint assays for comprehensive analysis. For example, in neural chips, although multichannel MEAs can record neuronal firing patterns, further validation of neurodegenerative changes still relies on immunofluorescence staining[35]. With the advancement of on-chip sensor integration, developing multimodal sensing technologies tailored to the specific pathological mechanisms of each model not only overcomes the limitations of single-parameter sensing but also bridges the gap between dynamic functional changes and molecular mechanisms.

In OoC platforms, multimodal sensing aims to obtain multidimensional and multiscale analysis of biological systems by integrating diverse sensing technologies, so as to enhance the depth of comprehension. Multidimensional integration indicates simultaneously monitoring of different functional parameters from the same biological behavior. For example, in cardiac function assessment, electrophysiological monitoring alone can only reflect cardiac rhythm, whereas the addition of mechanical sensing allows the simultaneous capture of contractile behavior[26,30,36–40]. Multiscale integration indicates sensing of the biological behavior at different level, including biomolecule level, tissue level, and the microenvironmental level, which aims to trace cross-hierarchical interactions and reveal causal relationships across different biological levels. For example, the induction of inflammatory factors released under hypoxic culture conditions, which subsequently compromised cellular barrier integrity[19,41]. Disruption of ion channel function at the molecular level can manifest as altered action potential duration at the tissue level, leading to impaired contractile function and metabolic imbalance, and ultimately causing changes in microenvironmental parameters[42–45].

This systematic multimodal sensing framework not only provides more comprehensive physiological data but, more importantly, establishes a complete causal chain from molecular events to tissue functions, advancing OoC research from observational studies toward mechanistic understanding. In the future, the deep integration of these two strategies is expected to offer a more powerful technological platform for drug development and disease modeling.

Monitoring targets in OoC systems

To construct a continuous monitoring system, the first priority is to clearly define the "target of monitoring." The monitoring objectives in OoC systems can be categorized at three levels from the microscopic to the macroscopic level: biomolecules, cellular/tissue behaviors, and the

Table 1 Organ-Specific In Vitro Tissue Models: Summary by Core OoC Scenarios with Detection Requirements

Organ	Tissue Model	Key Indicators	Parameter Range	Normal Tissue	Requirements	On-chip Detection Methods	Ref.
Heart	Drug-induced cardiotoxicity	FP/AP; Contractile force	1–2 Hz, 0.5–4 mV 0–50 μN	1 Hz, 2±0.5 mV 10–30 μN	High temporal resolution; Multi-point synchronization	Microelectrode array Strain sensor	23–30
	Myocardial infarction	miRNA expression	2 pM–10 nM	<5 pM	Rapid response; High sensitivity; High specificity	Electrochemical biosensor	66
Liver	Drug-induced hepatotoxicity	Human serum albumin GST-α	0.01–100 ng/mL 0.01–50 ng/mL	35–50 ng/mL <5 ng/mL	Dynamic Reusable	Electrochemical biosensor Optical biosensor	61,72
	Liver injury	GST-α; TGF-β	20–500 ng/mL LOD: 1ng/mL	/	Real-time; High sensitivity; Anti-interference	Optical biosensor Electrochemical sensor	33,34
Kidney	Drug-induced nephrotoxicity	Oxygen consumption rate (OCR); Metabolic process	13.21 nmol/min/10^6 cells	8–10 nmol/min	Embeddable Real-time	Optical sensor Electrochemical sensor	31
	Diabetic nephropathy	TEER; pH	200–350 Ω·cm^2 6.8–6.5	450–500 Ω·cm^2 7.2–7.4	Label-free; High sensitivity;	Microelectrode Optical sensor	204
Nerve	Drug-induced neurotoxicity	Mean firing rate (MFR); Burst parameters	MFR increase: 66–194% Burst number and frequency increased	10.1±6.2 Hz (31%)	Multi-channel	Microelectrode array	32
	Epilepsy	Neuron spike frequency	1–100 Hz	0.5–5 Hz	Multi-channel Long-term stable environmental control	Microelectrode array	212
	Alzheimer's disease	Positive and negative spike interval; Neural network synchronous discharge	Interneurons<500 μs Pyramidal neurons>700 μs	>800 μs	Multi-site dynamic	Microelectrode array	35
Lung	Pulmonary fibrosis	Alveolar deformation degree	75–140 μm	100–120 μm	Dynamic visualization	Optical strain sensor	107
	Pneumonia	IL-1β IL-6	1.5 ng/mL~1 μg/mL 7.6 ng/mL~1 μg/mL	<0.5 ng/mL	Label-free High-sensitivity Real-time dynamic	Optical biosensor	75
Intestine	Inflammatory bowel disease	TEER	200 ~ 260 Ω cm^2	350-400 Ω·cm^2	Label-free	Microelectrode	213,214

Table 1 continued

Organ	Tissue Model	Key Indicators	Parameter Range	Normal Tissue	Requirements	On-chip Detection Methods	Ref.
Blood Vessel	Hypertension	ROS	LOD:1.0×10^{-6} M	$<10^{-7}$ M	Stretchability	Electrochemical biosensor	57
		NO	LOD:1.6×10^{-9} M	$>10^{-8}$ M	Real-time dynamic		
	Thrombosis	Hardness	7.65–14.41 MPa	/	Bendable	Optical strain sensor	215
		Location			Real-time		
		Degree of occlusion					
Islet	Diabetes	OCR;	0.017–0.037 mol $m^{-3}s^{-1}$	0.025–0.030 mol:m^{-3}·s^{-1}	Real-time	Optical biosensor	73,216,217
		Insulin secretion	0.5–15 μg/mL	1.0–3.0 μg/mL			
Joint	Osteoarthritis	Glucose;	LOD:1.1 mM	4.5–5.5 mM	Long-term stable	Electrochemical biosensor	218,219
		Lactic acid;	LOD:0.6 mM	0.5–1.5 mM	Wide dynamic range	Optical biosensor	
		Fibrosis degree	5.9±0.25 V	4.0±1.2 V	High sensitivity		

Table 2 Summary of various biomarker in organ-specific models

Organ-Specific Models	Biomarker Detection	Ref.
Liver	TGF-β; GST-α; Albumin	33,34,220
Heart	miRNA; Cardiac troponin; CK-MB	221,222
Blood Vessel	ROS; NO	57,223,224
Muscle	TNF-α; IL-6	48
Nerve	Aβ1-42; p-Tau181; ACh; ROS	35,225
Lung	IL-1β; IL-6	75
Islet	Insulin	216

microenvironment, forming a comprehensive framework for assessing organ functionalities.

Biomolecules

Molecular detection can reveal the biochemical signaling mechanisms by which cells release factors, and the measurement of biomarkers enables accurate assessment of the status of ex vivo tissues and cellular functions such as metabolic activity and drug response. Due to its high specificity and sensitivity, ELISA remains the gold standard for biomarker quantification. It relies on the specific binding between antigens and antibodies, with enzyme-catalyzed colorimetric or fluorescence reactions enabling both qualitative and quantitative analysis of target molecules[46,47]. Table 2 summarizes OoC models requiring biomolecular detection and commonly used biomarkers for different organ systems. Compared with static, offline analyses[48–53], online monitoring allows continuous real-time measurement of key physiological parameters through the in situ integration of biocompatible sensors within OoC systems, eliminating the need for frequent sampling that may disrupt the microphysiological environment. To this end, in situ biosensing technologies based on electrochemical and optical mechanisms have become essential tools for real-time biomarker tracking. These sensors are readily integrable with microfluidic platforms and can monitor dynamic physiological processes within tissues. Fig. 1.

Electrochemical biosensing

Electrochemical sensors can convert biochemical events into measurable electrical signals. By immobilizing target biorecognition molecules on the electrode surface, interactions between the analyte and the electrode induce changes in current or potential[54]. Compared with other biosensing systems, electrochemical sensors offer excellent limits of detection (LOD) and response speeds, and are easily integrable with OoC platforms, enabling in situ and continuous monitoring of relevant biomolecules. Fig. 2.

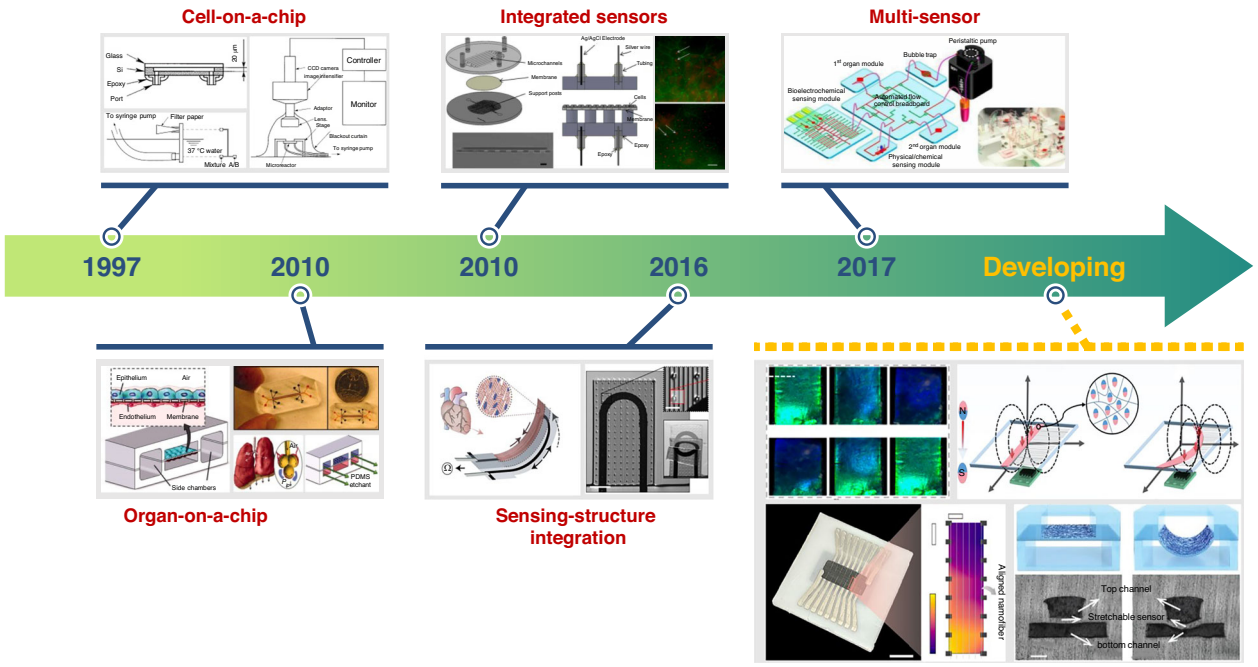

Fig. 1 Timeline of On-Chip Sensor Integration in Organ-on-a-Chip Systems[3–5,20–22]

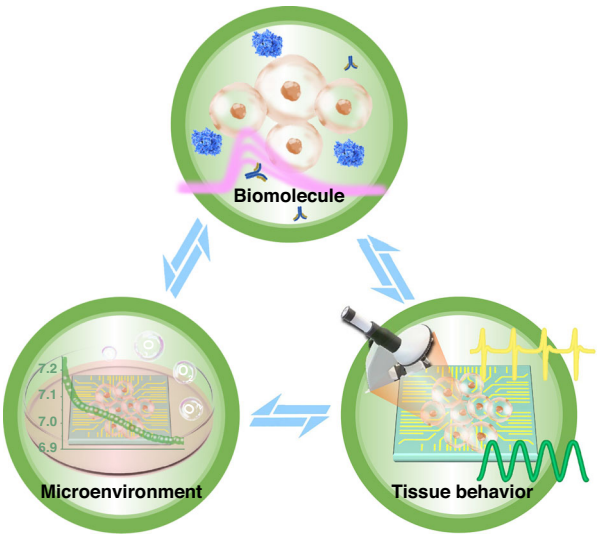

Fig. 2 Multimodal sensing technologies in OoC

Amperometric sensor is a commonly used biosensor for detecting electroactive species by applying a potential between the working and reference electrodes and measuring current generated during electrochemical reactions at the working electrode. A third counter electrode often improves reference stability[55]. Due to their simplicity and low LOD, amperometric sensors were widely used in biocatalytic and affinity-based sensing. In liver-on-a-chip systems, immobilized glucose oxidase catalyzed glucose oxidation to H_2O_2, enabling metabolic monitoring via current signals[16]. Similarly, Kidney-on-a-chip platforms similarly detected glucose and lactate, revealing a 6% increase in glucose uptake and a 37% decrease in lactate after cyclosporine exposure[31]. Ortega et al. functionalized gold electrodes with antibodies for in situ detection of TNF-α and IL-6 in muscle-on-a-chip models, achieving LOD of 8 ng·mL^{-1} and 2 ng·mL^{-1}, respectively[56]. To demonstrate that electrochemical sensors can simultaneously capture dynamic biochemical signals from blood vessels under mechanical stretching and drug treatment, Jin et al. developed a flexible sensor integrated onto the PDMS membrane of a vascular-on-a-chip system (Fig. 3a). By monitoring the oxidative currents of NO and ROS in real time, this sensor successfully revealed the rapid signaling responses of endothelial cells under stress stimulation. The LODs reached 1.6 nM for NO and 1 μM for ROS, marking the first simultaneous monitoring of vascular strain and biochemical signaling[57]. Another strategy used aptamers immobilized on electrodes, where target binding induced measurable current changes. In a liver injury model, a TGF-β aptamer-modified gold electrode was placed near the cell culture chamber. TGF-β secreted by hepatocytes under alcohol-induced injury bound to the aptamer, altering the distance between the redox probe (methylene blue) and the electrode, enabling real-time amperometric tracking of TGF-β[34]. The Revzin group applied the same approach to dynamically monitor theinterferon-γ via aptamer-induced redox current changes[58,59].

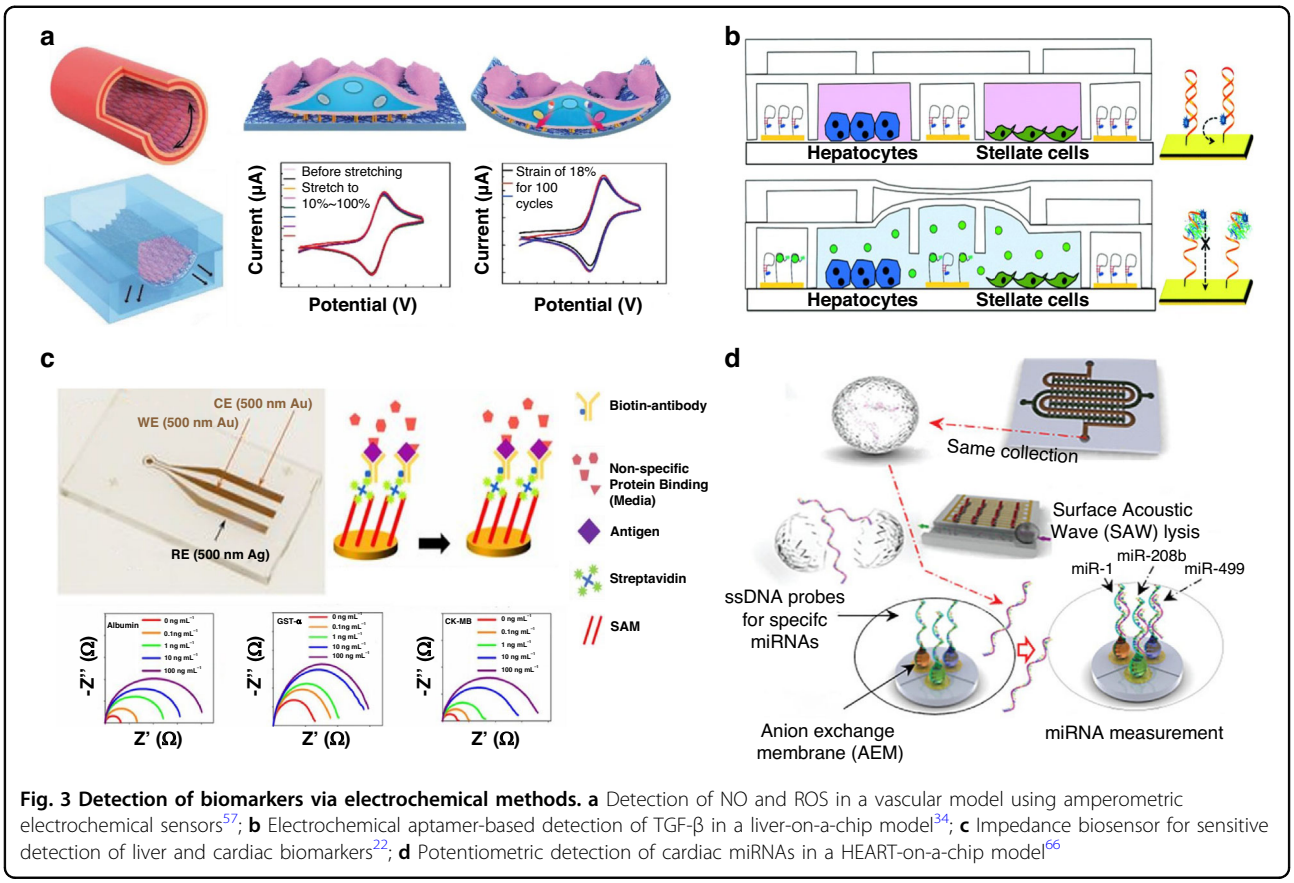

Fig. 3 Detection of biomarkers via electrochemical methods. a Detection of NO and ROS in a vascular model using amperometric electrochemical sensors[57]; **b** Electrochemical aptamer-based detection of TGF-β in a liver-on-a-chip model[34]; **c** Impedance biosensor for sensitive detection of liver and cardiac biomarkers[22]; **d** Potentiometric detection of cardiac miRNAs in a HEART-on-a-chip model[66]

Electrochemical impedance spectroscopy (EIS), first introduced by Lorenz and Schulze in 1975, can be used to monitor immunorecognition events, such as antibody–antigen binding on the electrode surface[60]. By measuring changes in the interfacial impedance between the electrode and the solution, the concentration of target biomarkers can be inferred. The core principle involves using EIS to monitor variations in the charge transfer resistance (R_{ct}), which increase when target molecules (such as human albumin or GST-α) bind to antibodies immobilized on the electrode surface. In a study by Shin et al., EIS-based detection of albumin achieved a LOD as low as 0.023 ng/mL, outperforming traditional ELISA methods, which typically reach an LOD of 0.2 ng/mL[61]. Impedance biosensors apply an alternating current potential between electrodes to measure changes in the impedance of the medium, serving as a powerful tool for detecting variations in interfacial properties at the electrode surface. In Fig. 3c, Zhang et al. functionalized gold electrodes with 11-mercaptoundecanoic acid, a streptavidin layer, and biotinylated antibodies. The resulting impedance biosensors achieved LOD of 0.01 ng mL^{-1} for GST-α, 0.09 ng mL^{-1} for albumin, and 0.0024 ng mL^{-1} for CK-MB[22].

Potentiometric sensors measure the concentration of target analytes by detecting potential change across selective membranes. These changes arise from specific interactions between target molecules and recognition elements, which alter local charge distribution or ion mobility at the interface[60]. They are commonly used to monitor ion concentrations[62,63]. For example, ion-selective electrodes detect potential differences generated by specific ion accumulation, enabling reagent- and label-free measurement[64]. Since neuronal function depends on ion flux (e.g., Na^+, K^+, Ca^{2+}, Cl^-), extracellular ion changes can indicate dysfunction[65]. Bradley developed a HEART-on-a-chip model (Fig. 3d) incorporating a potentiometric sensor with an anion exchange membrane for miRNA detection and a surface acoustic wave lysis module. Each AEM sensor measurement takes less than 30 min and allows for dynamic sampling at 1 hour of ischemia and 1 hour of reperfusion, capturing real-time fluctuations in miRNA concentrations[66].

Electrochemical biosensors offer rapid response times and are easy to integrate, but require direct contact between the electrodes and the sample during detection.

Optical biosensing

Optical sensing platforms offer complementary approaches for biomolecular detection. Optical biosensors provide information on molecular interactions by

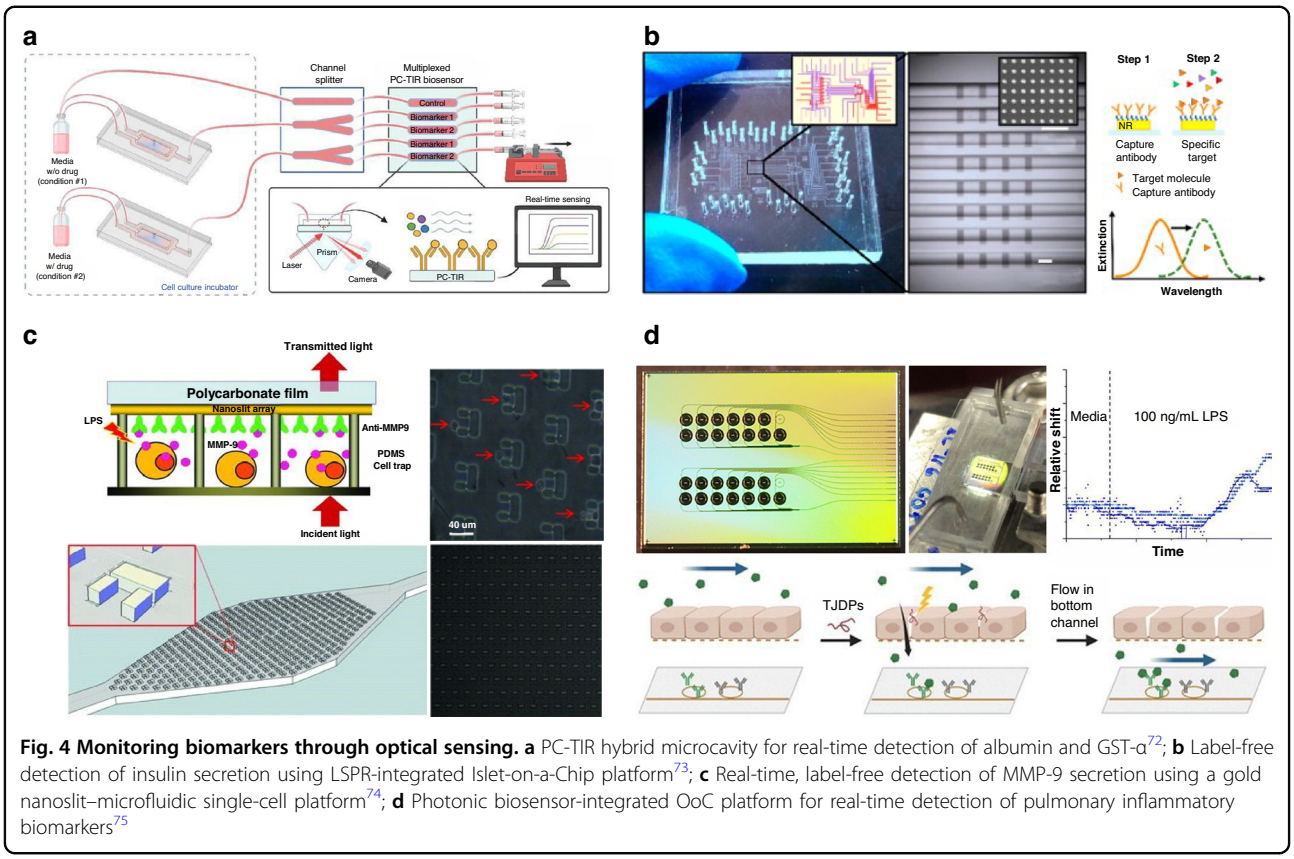

Fig. 4 Monitoring biomarkers through optical sensing. a PC-TIR hybrid microcavity for real-time detection of albumin and GST-α[72]; **b** Label-free detection of insulin secretion using LSPR-integrated Islet-on-a-Chip platform[73]; **c** Real-time, label-free detection of MMP-9 secretion using a gold nanoslit–microfluidic single-cell platform[74]; **d** Photonic biosensor-integrated OoC platform for real-time detection of pulmonary inflammatory biomarkers[75]

monitoring changes in light intensity, refractive index, and the angle of incident/reflected light. Optical biosensors are predominantly engineered based on the principle of surface plasmon resonance (SPR). SPR occurs when the phase of the surface plasmon wave matches that of the evanescent wave[67–69]. When the wavelength of the incident light is fixed, a resonance angle that is highly sensitive to changes in the refractive index can be determined. By measuring the shift in the resonance angle, the interactions between ligands and analytes on the sensor surface were detected[70,71].

In Fig. 4a, Yang et al. developed a PC-TIR integrated liver-chip platform featuring an open optical microcavity formed by a 1D photonic crystal (TiO_2/SiO_2 multilayers) and total internal reflection interface. Biomolecular binding to surface-immobilized antibodies alters the refractive index of the microcavity, inducing resonance angle shifts in reflected light. Quantitative label-free detection is achieved by tracking these angular deviations. The system enabled detection of albumin across a range of 21.7 ng/mL to 7.83×10^3 ng/mL and GST-α from 2.20 ng/mL to 7.94×10^2 ng/mL, with LOD of 21.68 ng/mL and 2.20 ng/mL, respectively. Thereby meeting the requirements for monitoring physiological concentration levels. Response times reached ~277 s for albumin and ~209 s for GST-α, enabling capture of drug-induced early-stage secretion dynamics[72]. Integrated Localized Surface Plasmon Resonance (LSPR) sensing technology coupled with Islet-on-a-Chip (IOC) devices utilized gold nanorod structures (shown in Fig. 4b). Changes of refractive index due to biomolecular binding in the surrounding medium caused peak wavelength shifts in the LSPR spectrum. Label-free detection was accomplished by monitoring shifts in wavelength or intensity variations. This system achieved in situ monitoring of insulin secretion from pancreatic islets, with a LOD of 0.85 ± 0.13 μg/mL, making it suitable for trace-level insulin quantification[73].

Figure 4c illustrates an innovative optical platform designed for real-time, label-free monitoring of single-cell secretions. At the core of this system is a gold nanoslits array, whose Fano resonance is highly sensitive to changes in surface refractive index. The key advantage of this design lies in its integration of high-sensitivity optical sensing with single-cell capture microfluidics, enabling a direct correlation between secretion activity and individual cells. As shown, when MMP-9 secreted by THP-1 cells binds to antibodies on the sensor surface, the resonance wavelength shifts, compellingly demonstrating that this platform can quantitatively track single-cell secretion dynamics without the need for labels. Quantitative analysis revealed that each cell secreted an average of 0.7 pg

of MMP-9 over a 13 h culture period, consistent with ELISA validation, while reducing cell consumption by approximately four orders of magnitude[74].

Label-free optical sensing leverages intrinsic light-matter interactions to eliminate fluorescent tagging or molecular labeling. This noninvasive nature preserves native cellular physiology, thus enabling longitudinal real-time monitoring throughout extended culture periods. Cognetti et al. developed an OoC platform integrated with photonic biosensors, embedding silicon nitride microring resonators within a dual-channel microfluidic system for real-time monitoring of pulmonary epithelial inflammatory biomarkers, as shown in Fig. 4d. Analyte binding to surface-immobilized antibodies altered the effective refractive index surrounding the resonators, inducing resonant wavelength redshifts. Quantitative detection was achieved by measuring these spectral shifts. Using human bronchial epithelial cells stimulated by lipopolysaccharide, the photonic sensors detected secreted IL-1β (LOD: 1.5 ng/mL) and IL-6 (LOD: 7.6 ng/mL) within 1 h[75].

Challenges in biomolecular monitoring

In OoC experiments that can last for several weeks, cells continuously secrete proteins and deposit extracellular matrix during this period, while the sensing interface functionalized with probes remains static and non-adjustable[61,72]. Many high-sensitivity sensors are prone to saturation when the target concentration is excessively high, whereas an overly broad dynamic range may compromise sensitivity. This mismatch between the static interface and the dynamic biological system poses a critical challenge for real-time monitoring of molecular concentration changes[31,33,34].

It is difficult to enable dynamic monitoring both real-time and selective, due to the irreversible binding characteristics of traditional antibody probes. Therefore, developing novel reversible aptamer probes is essential to enable truly continuous monitoring[76–78]. In addition to reversible probes, optimizing the sensor interface design by reducing non-specific protein adsorption enables efficient recognition in complex media, thereby enhancing sensor stability and selectivity under physiological conditions[79,80].

Cell/tissue behavior

The detection of biomolecules solely reflects chemical-level alterations, while assessing the functional status of cells/tissues requires behavioral-level indicators including mechanical activity and electrical signaling. Visual observation constitutes the fundamental approach for evaluating cellular morphology and tissue architecture in OoC platforms[81], supported primarily by microscopy and high-content imaging[82–85]. Most devices maintain compatibility with epifluorescence or confocal microscopy, with high-content imaging additionally capturing spatiotemporal information of 3D multicellular architectures to facilitate correlation analysis between structural features and pathological mechanisms[86–88]. Comprehensive investigation of cellular/tissue behaviors necessitates integrated sensors for multimodal monitoring. As core manifestations of organ functionality, mechanical activity, electrical signaling, and barrier function are introduced in this section.

Mechanical activity

Mechanical activity represents the most direct manifestation of tissue functional status. Strain sensors enable real-time monitoring of mechanical signals from cellular contractions and tissue deformations in OoC. These sensors convert resulting deformations into quantifiable electrical or optical signals, encompass strength of contractile force, rhythmicity, and ratio of contraction and relaxation in cardiomyocytes.

Piezoresistive strain sensors convert strain variations into corresponding changes in electrical resistance[21,89,90], For example, in one design, elastic microfluidic channels were filled with liquid metal, and the deformation of the membrane induced by myocardial tissue contraction elongates the liquid metal path, increasing resistance (Fig. 5a). These embedded liquid metal sensors are connected to external circuits via a Wheatstone bridge to collect resistance and voltage signals, By employing a Wheatstone bridge design and a built-in temperature compensation mechanism, the sensor outperforms single-arm configurations in terms of sensitivity, linearity, repeatability, and stability, effectively addressing performance limitations caused by the temperature sensitivity of liquid metal[91]. Crack-based sensors also represent a typical strain detection technique utilizing the piezoresistive effect[28,92]. Wang et al. proposed an Ag/CNT-PDMS crack sensor in which cardiomyocyte contraction causes bending-induced cracks in the silver layer, illustrated in Fig. 5b. The silver islands are bridged by CNTs embedded in the PDMS, effectively suppressing crack propagation and significantly improving the stability of the crack sensor. The separation and reconnection of silver islands lead to rapid changes in the conductive network, resulting in a gauge factor on the order of 10^5, an operating strain range of 0.01% to 44%, and the signal-to-noise ratio (SNR) increased to 73.4, all of which significantly surpass the performance of commercial silicon strain gauges[93]. Parker's team employed multi-material 3D printing to embed CB:TPU strain gauges within a cantilever structure, converting the stress generated during tissue contraction into measurable resistance changes. Within a strain range of 0.1%, the sensor exhibits a linear fit of $R^2 = 0.99$ for relative resistance change. This excellent linearity ensures accurate conversion from resistance signals to mechanical stress, providing a foundation for the quantitative analysis of myocardial contractile strength[21].

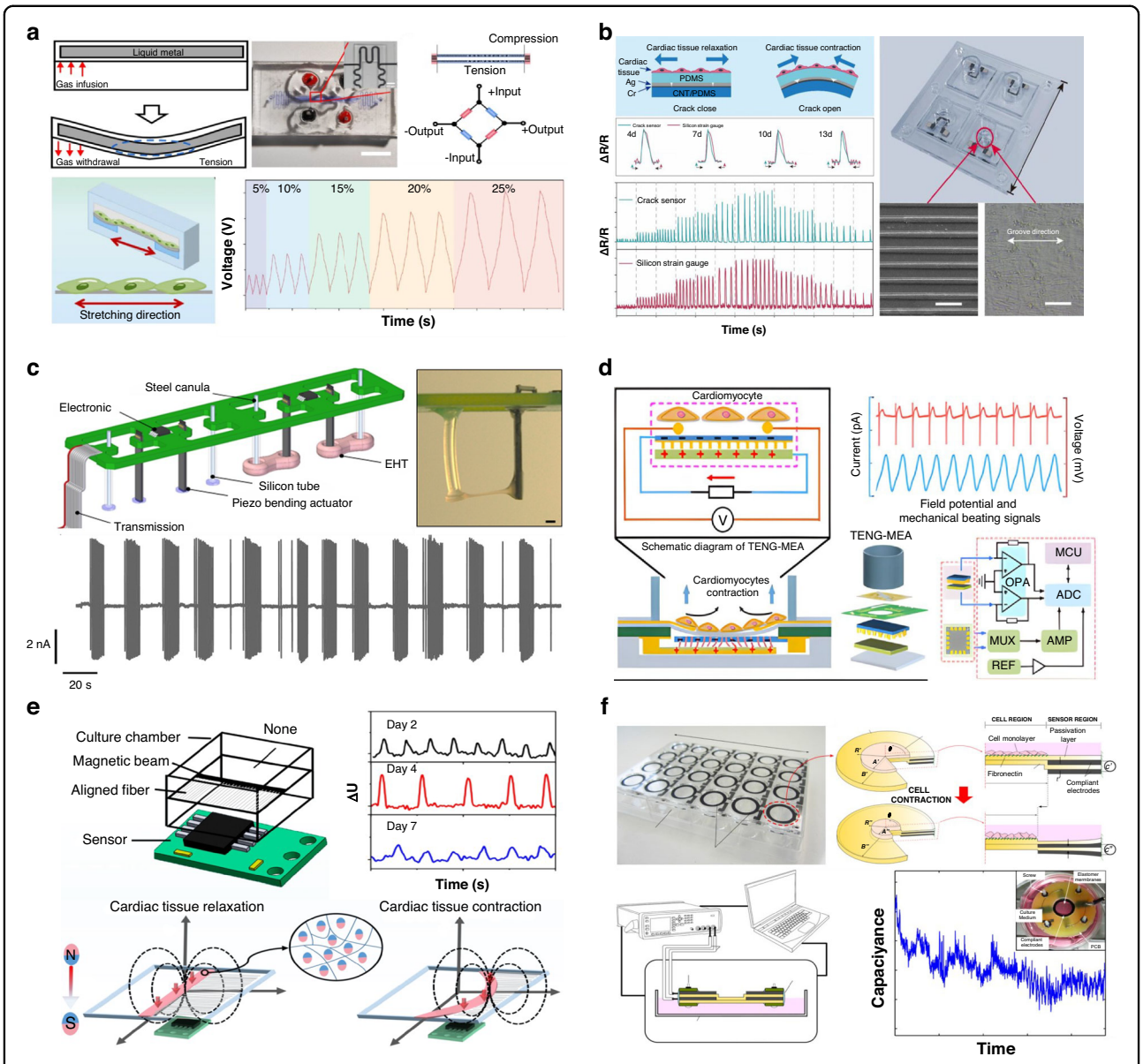

Fig. 5 Electrical signal-based detection of tissue mechanical stress. a Embedded liquid metal sensors for real-time monitoring of myocardial tissue contraction[91]; **b** Ag/CNT-PDMS crack-based strain sensor for monitoring cardiomyocyte contraction; **c** Piezoelectric sensing of cardiac tissue contraction using PDMS pillar-based anchoring[95]; **d** Triboelectric-based cardiac contraction sensing using a variable-gap nanopillar design[99]; **e** Magneto-responsive platform for cardiomyocyte contractility sensing using magnetoresistive detection[29]; **f** Capacitive sensing of smooth muscle cell contraction using a parallel-plate design[100]

Piezoelectric materials generate a relative potential difference upon deformation, enabling the detection of mechanical forces exerted by tissues in vitro[94]. For example, cardiac tissue can be anchored to hollow elastic PDMS pillars, where tissue contraction induces deformation, causing the piezoelectric sensing unit on the pillar to generate a measurable current[95]. Nguyen et al. employed $PbZr_xTi_{1-x}O_3$(PZT) nanoribbons to detect mechanically induced deformations of cells in response to electrical stimulation. When transferred onto cyclically deforming lung tissue at a macroscopic scale, these piezoelectric nanoribbons generated voltage outputs on the order of 0.5 V and current signals in the nanoampere range[96]. Electrospun polyvinylidene fluoride piezoelectric fiber mats have also been developed to offer support for cell adhesion and growth while exhibiting mechanical responsiveness, thereby enabling real-time monitoring of cardiomyocyte contractions[97]. In recent years, triboelectric nanogenerators have been widely applied for monitoring subtle mechanical stimuli, and some

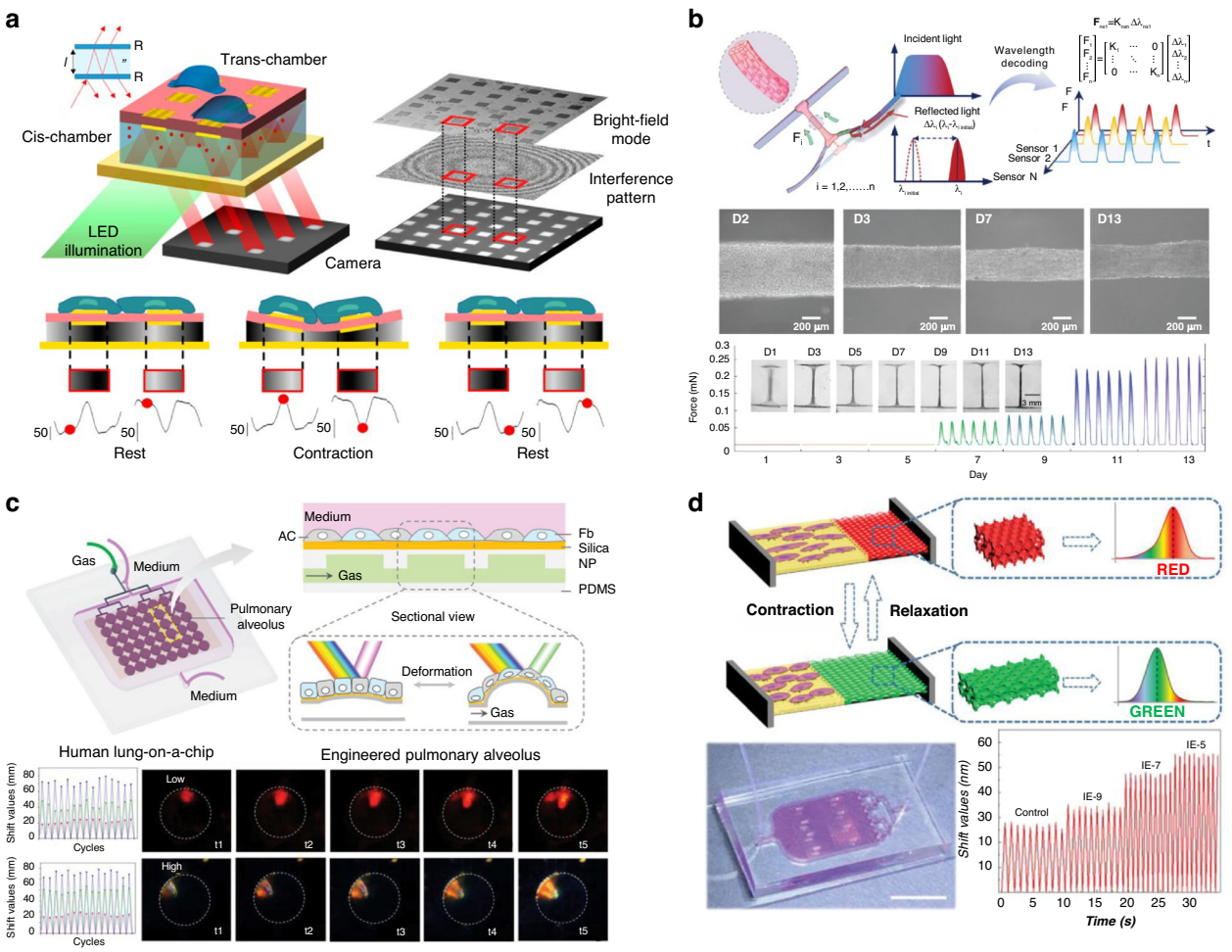

Fig. 6 Mechanical strain detection in tissues using optical responses. a Label-free interferometric imaging of cardiomyocyte contraction using an optical interferometer array[101]; **b** Real-time monitoring of cardiac tissue contraction using fiber Bragg grating (FBG) sensors[102]; **c**, **d** Real-time tissue dynamics tracking via structural color biosensors[103,107]

researchers have explored their use in detecting cardiac tissue contractions [98]. As illustrated in Fig. 5d, Zhang et al. introduced a variable-gap design between vacuum-compressed nanopillars and a fluorinated ethylene propylene triboelectric layer. During cardiomyocyte contraction, periodic contact and separation between the triboelectric layers generated alternating charging/discharging cycles. The system demonstrated a contraction detection sensitivity of 1.146 pA/Pa and a SNR of up to 43.1 dB[99].

Mechanical deformation can also be transduced electromagnetically or electrostatically, enabling electrical readout of tissue-level mechanical activity, Sun's team developed a magneto-responsive mechanical sensing platform by integrating nanofibers with magnetic cantilevers, which converts cardiomyocyte contractile forces into voltage variations via magnetoresistive sensors (as shown in Fig. 5e), achieving a LOD of ~6 μN for contractile force[29]. Capacitive sensing provides an alternative approach for measuring cellular contraction forces by detecting changes in capacitance within the sensing region. In Fig. 5f, Araromi et al. developed a capacitive sensor based on a parallel-plate capacitor, in which contraction of smooth muscle cells alters the dimensions of flexible electrodes in the sensing region, thereby changing the capacitance. This device can detect a minimum contractile stress of 1.2 kPa from the cells[100].

Optical detection provided new insights and methodologies for the measurement of tissue-level mechanical activity. Shown in Fig. 6a, Boschi proposed a label-free, high-resolution imaging method based on an optical interferometer array to monitor the contraction of hiPSC-derived cardiomyocytes (hiPSC-CMs) in vitro. Owing to the sensitivity of interferometric techniques, displacements as small as tens of nanometers can be detected at multiple locations simultaneously[101]. The conversion of

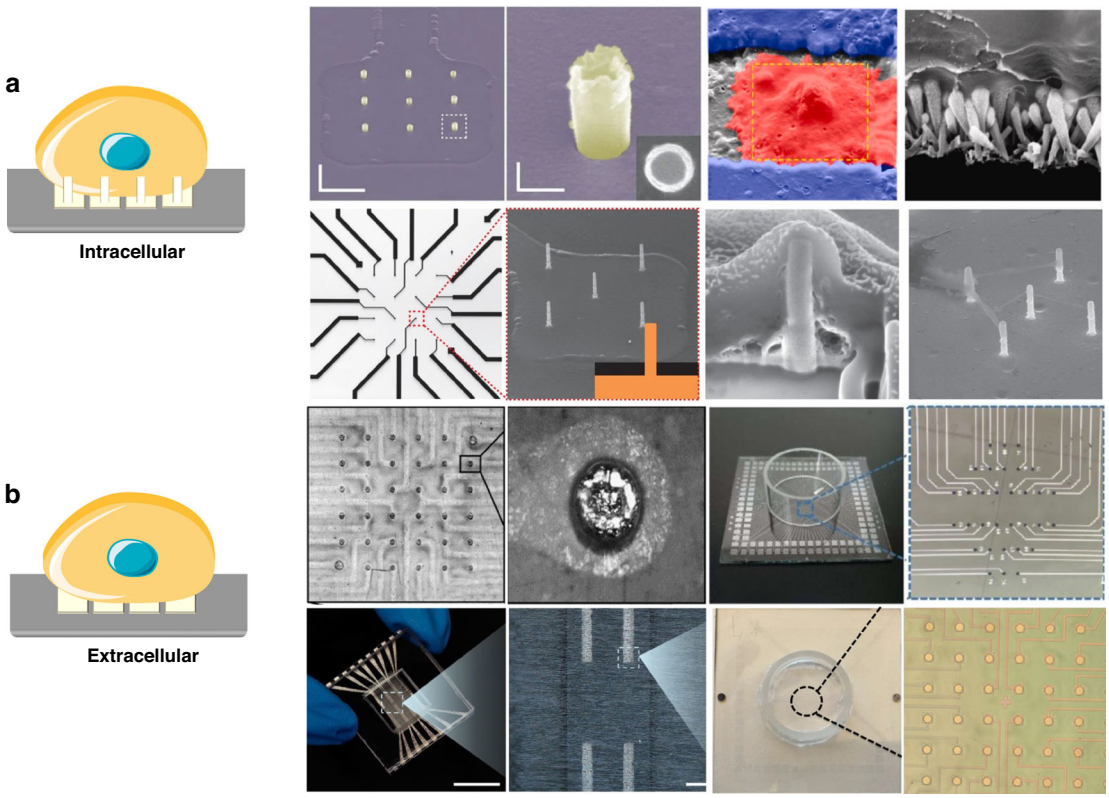

Fig. 7 Comparison of intracellular and extracellular electrophysiological recordings. Electrophysiological recording encompasses both intracellular (**a**)[116,117,121] and extracellular (**b**)[35,132,183,226] methodologies, capturing action potentials and field potentials, respectively

tissue deformation into optical signal changes can also be achieved using fiber Bragg grating (FBG). In relevant studies, cardiac tissue contraction generates forces that induce displacement of a suspended optical fiber, leading to a shift in the central wavelength of the FBG (Fig. 6b). By pre-calibrating the sensor to establish the relationship between wavelength shift and contractile force, real-time monitoring of human engineered heart tissue contraction has been achieved with a sensitivity of up to 117.5 pm·mN^{-1}. Under drug stimulation, FBG-based fiber sensors have demonstrated the capability for multi-channel detection, long-term, and real-time monitoring of contractile responses[102]. Structural color materials have also provided a new approach for monitoring dynamic tissue changes[103–106]. Zhao et al. developed structurally colored PDMS and applied it to a lung-on-a-chip model with visualized respiratory function (Fig. 6d), using mechanochromic responses to explore the phenotype of idiopathic pulmonary fibrosis[107].

Electrical activity

Bioelectrical activity is a critical function of excitable cells such as cardiomyocytes and neurons. In OoC, in situ monitoring of electrical activity focuses on two fundamental types of bioelectrical signals generated by excitable cells: action potentials (AP) and field potentials (FP). AP represent rapid, propagating changes in the membrane potential of individual cells, encompassing the full process of depolarization and repolarization (e.g., cardiomyocyte APD90)[108,109]. These signals directly reflect ion channel function, cellular excitability, and drug-target interactions[110]. In contrast, field potentials are the summation of extracellular voltage changes arising from the synchronized firing of cell populations, capturing tissue-level electrical conduction efficiency, network synchrony, and pathological rhythmicity[111,112]. The patch-clamp technique remains the “gold standard” for intracellular recordings, capable of capturing high-fidelity single-cell action potential waveforms[113]. Traditional patch-clamp techniques have evolved into integrated systems and are widely applied in biomedical research[114]. However, the irreversible damage to cells and the complexity of the procedure limited its suitability for long-term recordings. Fig. 7.

With advances in micro- and nanofabrication technologies, the broad selection of materials and flexible structural designs has laid a feasible foundation for intracellular electrophysiological recordings. Electrode geometry critically governs cell-device coupling efficacy. To minimize interfacial gaps, Hai et al. pioneered a bioinspired 3D electrode replicating dendritic spine

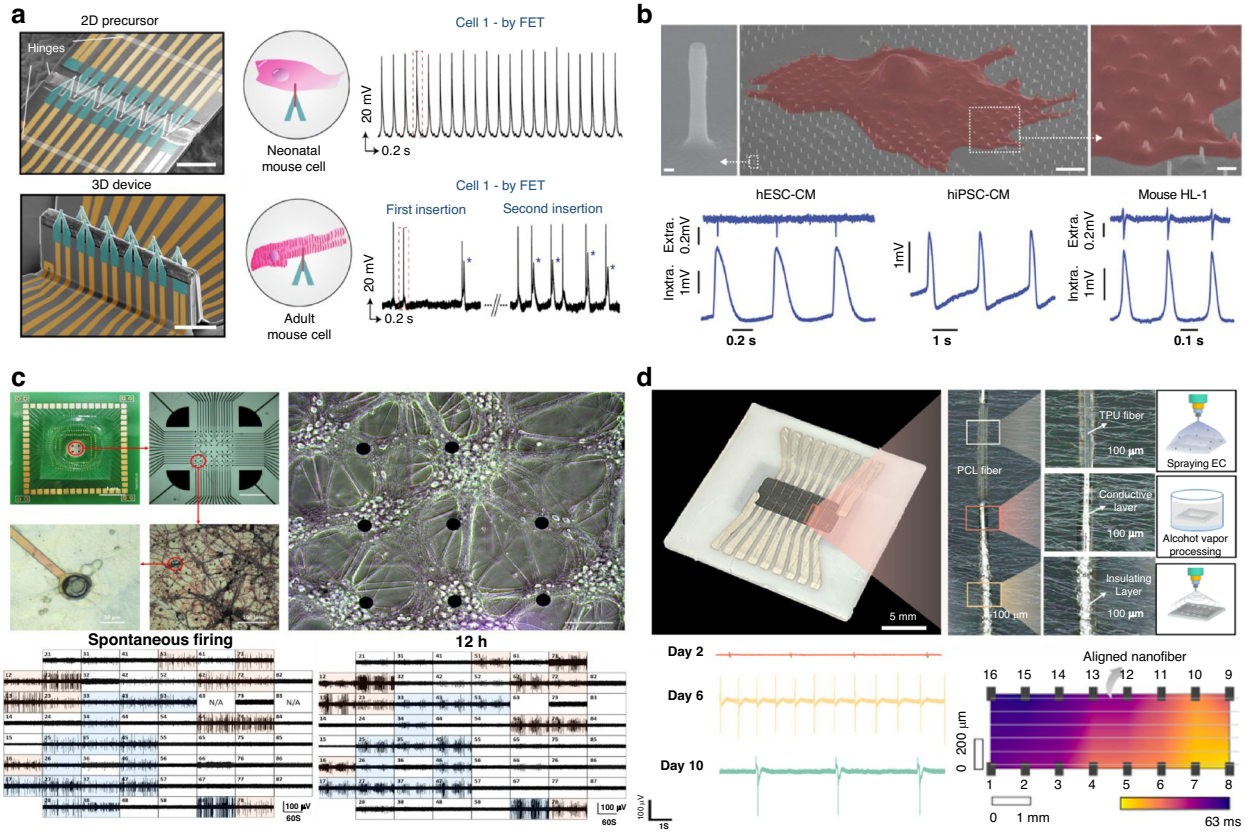

Fig. 8 Nanostructured electrodes for intracellular electrophysiological recording. a Buckled NanoFET Array for Minimally Invasive Intracellular Electrophysiology[123]; **b** Pt nanoelectrode array capturing prolonged action potentials; Whereas planar microelectrode arrays enable tissue-level electrophysiological signal monitoring: **c** MEA-based detection of AD-related neural dysfunction and in vitro neuromodulation therapy[35]; **d** Direction-resolved electrophysiological mapping in engineered cardiac tissue via fiber-aligned suspended MEAs[112]

morphology and scale, demonstrating enhanced cell-electrode coupling fidelity[115]. Further advancing intracellular recording capabilities, one-dimensional nanomaterials and nanostructures have been strategically implemented to optimize cell membrane penetration performance[116–119]. Lieber's group pioneered kinked nanowire and branched nanotube bio-probes featuring source/drain terminals and nanoscale field-effect transistor (FET) channels to achieve signal amplitudes comparable to patch clamp recordings. Free from interfacial impedance constraints, these nanostructures enable electrode miniaturization for high-density nanoelectrode arrays. Furthermore, their nanoscale architecture critically modulates cell-electrode coupling efficiency and intracellular access pathways[120]. Notably, hollow tubular electrodes functionally delay membrane resealing and induce active membrane fusion, thereby enhancing seal resistance and sensor stability for prolonged intracellular recording[121,122].

Intracellular recording electrodes demonstrate substantial potential for advancing disease modeling. As shown in Fig. 8a, a scalable 3D FET array platform was fabricated using a compressive buckling technique, enabling minimally invasive interfacing with the cellular membrane. With its high spatiotemporal resolution, the platform measured intracellular signal propagation velocity in cardiomyocytes as 0.182 m/s[123]. Lin et al. developed an innovative platform using a vertical Pt nanoelectrode array to study hiPSC-CMs (Fig. 8b). This system successfully recapitulated the prolonged AP signature characteristic of long QT syndrome, validating its utility for disease-specific investigations[27]. Separately, Liu et al. engineered a heart-on-a-chip model integrating microfluidic channels, cell culture chambers, and embedded electrodes capable of dual-mode extracellular and intracellular electrophysiological monitoring. This platform comprehensively resolved hypoxia-induced alterations in cardiac electrical activity[109].

Microelectrode arrays (MEAs) were initially developed and widely used for extracellular recordings of cardiomyocytes and neurons[124–126]. Extracellular recording offered a cost-effective and time-efficient approach,

enabling non-invasive, long-term, and multiplexed electrophysiological measurements[127,128]. MEAs designed for recording extracellular field potentials have progressively evolved toward increased electrode density and count, aiming to enhance detection throughput and enable multi-site monitoring of in vitro tissue models[129,130]. For example, Cai's group used MEAs to investigate the relationship between neural bursts and local field potentials in neuronal cultures, demonstrating that modulation of single-neuron excitability can influence overall network activity. The integration of MEAs with neuronal cultures holded great promise as an effective in vitro brain model platform for applications such as drug screening, neurological disease research, and the exploration of neural function[131,132]. In an in vitro Alzheimer's disease model induced by Aβ oligomers, MEA were used to record two distinct firing patterns originating from interneurons and pyramidal neurons (Fig. 8c). Spatial firing pattern mapping and cross-correlation analysis between channels were performed to assess the degradation of neuronal network connectivity[35].

Similarly, in a heart-on-a-chip platform combining cardiac tissue with MEAs, Xue developed a suspended microelectrode array integrated with an aligned fibrous scaffold, which enabled the determination of both the propagation direction and velocity of electrophysiological signals in the cardiac tissue, as shown in Fig. 8d[112]. By leveraging substrate-induced self-curving, it is also possible to achieve multi-site, long-term, and high-resolution electrophysiological monitoring of 3D tissues. Kalmykov et al. employed a self-rolling structure that could encapsulate cardiac spheroids, enabling twelve microelectrodes to synchronously record FPs in 3D space with cellular-level spatial resolution. Using 12-channel synchronous recordings, they constructed 3D isochronal maps and calculated conduction velocity (averaging 12.45 ± 1.88 cm/s), thereby revealing the propagation direction and pathways of electrical signals within the spheroid[111].

Intracellular recording technologies, particularly bioinspired 3D nanostructures and penetrating nanoelectrodes, now enable high-fidelity, long-term action potential measurements at the single-cell level, overcoming the limitations of traditional patch clamping for disease modeling and drug response studies. Concurrently, high-density and flexible MEAs provide unparalleled capabilities for non-invasive, multiplexed mapping of field potentials across cellular networks and 3D tissues, revealing tissue-level conduction dynamics and network pathologies. Critically, a synergistic convergence between these two approaches is emerging, exemplified by dual-mode platforms capable of simultaneously capturing both intracellular APs and extracellular FPs, thus providing a comprehensive, multiscale view of bioelectrical activity[109,133].

Barrier function

Barrier integrity is essential for maintaining physiological function, and TEER is widely recognized as the gold standard for evaluating cellular barrier function on OoC. TEER directly reflected the integrity and functionality of tight junctions between cells and can be used to assess the completeness and permeability of any epithelial or endothelial barrier tissue[134]. Electrodes were typically integrated directly onto the chip to enable real-time, noninvasive monitoring of barrier function in various cell types, such as airway epithelial cells and intestinal epithelial cells[135,136]. Integrated electrodes enabled real-time monitoring of endothelial permeability, where shear stress alterations induced by endothelial inflammation prompt corresponding TEER variations[137]. BBB-on-a-chip studies utilize TEER values to validate barrier permeability of BBB endothelial cells[138,139], as demonstrated in Fig. 9b, an innovative microfluidic system incorporating thin-film electrodes enables non-invasive, real-time monitoring of BBB model maturation and integrity. This platform utilized EIS to measure impedance variations, coupled with equivalent circuit modeling to extract more accurate TEER values (17.83 ± 1.61 $\Omega \cdot cm^2$).

Barrier disruption often indicated the onset of pathological conditions. For instance, in a proximal tubule kidney model, TEER values were closely correlated with cisplatin-induced nephrotoxicity, demonstrating TEER's potential as a rapid, early, and label-free indicator of toxicity in vitro[140]. In cardiac tissue models, treatment with the inflammatory cytokine TNF-α led to endothelial barrier damage, with TEER dropping from 230 ± 45 Ω to 15 ± 13 Ω, fluorescence microscopy further confirmed severe barrier disruption[141]. Beyond detecting barrier impairment, TEER can also be used to monitor fibrosis development in microphysiological systems. For example, Choi et al. used TGF-β1 to induce cellular fibrosis and employed embedded TEER electrodes to monitor the progression of fibrosis in a liver-on-a-chip[142]. To investigate aging effects on intestinal barrier integrity, Konstanze et al. incorporated interdigitated gold electrodes into a gut barrier chip, facilitating continuous tracking of cell adhesion, proliferation, differentiation, and intestinal integrity. Following treatment with the senescence-inducing agent doxorubicin, the impedance sensors achieved real-time, non-invasive, and continuous monitoring of aging-induced intestinal barrier alterations (Fig. 9c)[143]. Beyond electrode-based detection, Schellberg et al. further utilized fiber-optic sensors to perform real-time monitoring of barrier function in models of intestinal inflammation and chronic vascular inflammation (Fig. 9d)[144].

Although TEER is a commonly used metric for evaluating biological barrier integrity, the thresholds indicating full barrier competence vary across different models. Sole reliance on TEER cannot accurately characterize barrier

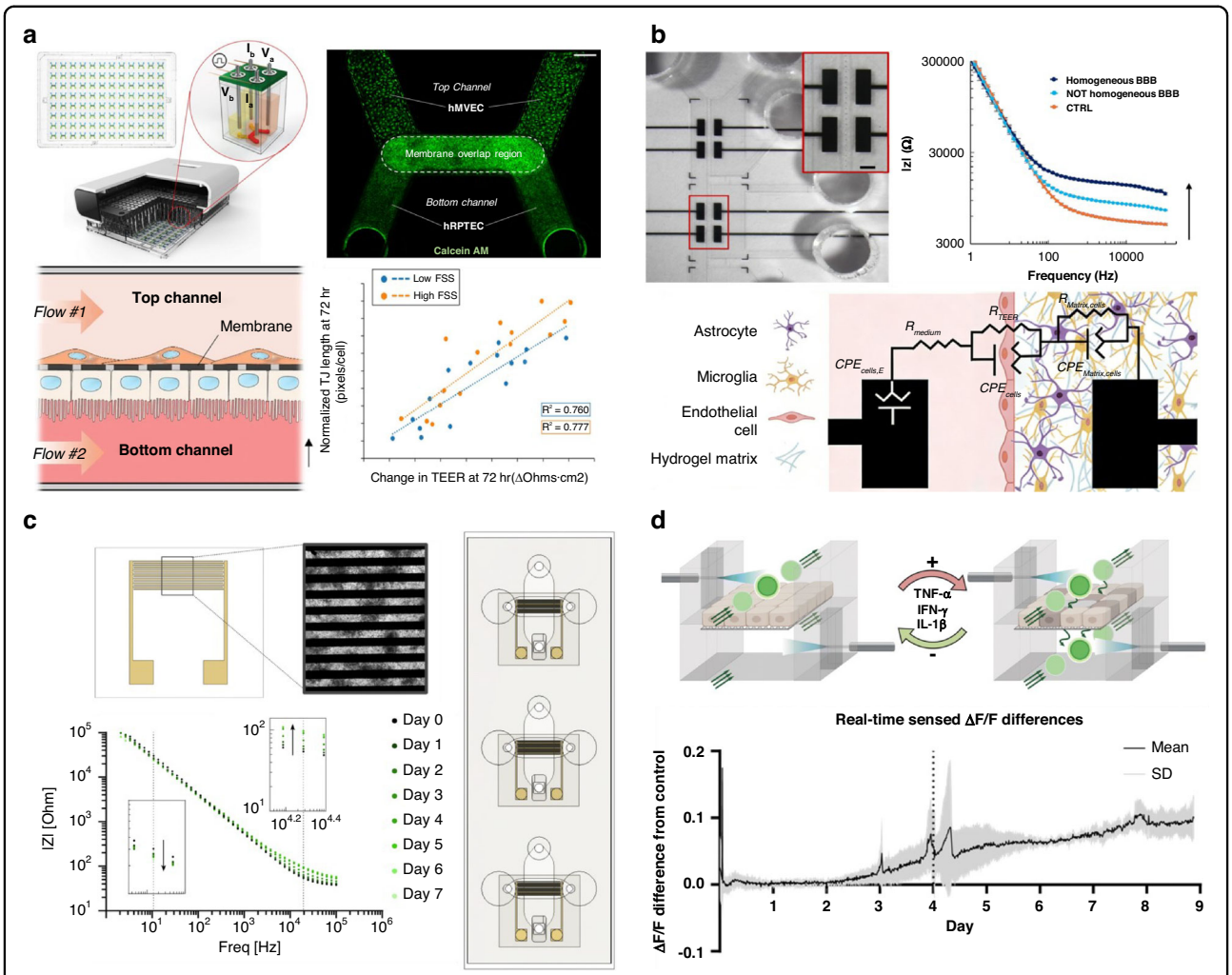

Fig. 9 Real-time monitoring of barrier function in various OoC using integrated biosensors. a Cisplatin-induced nephrotoxicity tracked in real time using TEER in a kidney-on-a-chip[140]; **b** Integrated thin-film electrodes enable real-time BBB maturation and integrity monitoring via EIS[139]; **c** Real-time impedance monitoring of aging-induced intestinal barrier dysfunction using a gut-on-a-chip[143]; **d** Fiber-optic sensor integration for dynamic assessment of epithelial and endothelial barrier integrity under inflammatory conditions[144]

maturation or functional integrity[139,145]. Therefore, comprehensive assessment of barrier status requires combining TEER with complementary methods (such as permeability assays and immunofluorescence validation).

Challenges in monitoring cell/tissue behavior

In monitoring cellular and tissue behaviors, a primary challenge lies in the mechanical modulus mismatch between sensors and soft tissues. Metallic sensing materials with excellent conductivity typically possess moduli far exceeding that of biological tissues, which can induce interfacial shear stress under dynamic loading, leading to device delamination or tissue damage[146]. One solution is by designing microscale mesh or porous architectures that enable macroscopic flexibility from high-modulus materials, allowing the sensor to integrate seamlessly with soft tissues such as organoids for long-term stable monitoring[147,148].

By employing high-density microelectrode arrays with subcellular resolution, it is possible to achieve electrical recordings at single-cell precision while maintaining the ability to monitor network dynamics at the population level[25,149]. Such high-density microelectrode platforms can also capture electrical pulses that occur during cell migration[150,151]. Correlating detailed electrophysiological features with cellular behavior patterns allows researchers to gain deeper insights into the relationship between electrical activity and cell function.

Microenvironment

Microenvironment monitoring serves as an essential complement to comprehensive functional assessment.

The microenvironment level refers to the physicochemical conditions surrounding cells, rather than signaling molecules actively produced by the cells, which include oxygen gradients, pH, fluid shear stress, temperature fluctuations and so on. Its function is to establish and maintain a physiologically relevant environment. By integrating advanced structural designs and bioengineering principles into microfluidic devices, precise biochemical and mechanical stimuli can be delivered, thereby simulating the complex microenvironment and physiological functions of human organs in vitro. To faithfully emulation and control actual physiological microenvironments, OoC platforms require real-time, dynamic monitoring and regulation of a range of critical environment parameters.

Mechanical microenvironment

The stiffness of the extracellular matrix (ECM) is a crucial physical parameter that directly affects normal cellular function[152]. A relatively simple detection method involved culturing hESCs on a polyacrylamide hydrogel embedded with fluorescent microbeads. By tracking the displacement of the beads, the traction forces exerted by the cells on the substrate were calculated, enabling analysis of both the magnitude and dynamic changes of forces within hESC colonies[153]. The Rahimi team designed an OoC platform utilizing ultrasound to measure the stiffness of cell culture matrices (Fig. 10a). This platform allowed in situ investigation of both static and transient mechanical properties of the ECM in on-chip 3D cell culture and tissue engineering applications[154].

During dynamic in vitro tissue culture, periodic mechanical stimulation[155–158] or fluid shear stress is often applied. Microfluidic technology enables the reconstruction of in vivo-like fluidic environments in vitro[159], allowing the generation of various types and patterns of shear stress within perfusion chambers. This makes it possible to study how shear forces influence cell growth and function[160,161]. For example, impedance sensors integrated into microfluidic systems allows real-time monitoring of the dynamic behavior of endothelial monolayers under fluid shear stress (Fig. 10c). By acquiring impedance spectra in the 100 Hz to 1 MHz frequency range, parameters such as transendothelial resistance, cell membrane capacitance, and medium resistance were used to assess cell permeability, adhesion, and environmental conditions[162]. To monitor the mechanical microenvironment composed of fluid shear stress and hydrostatic pressure in real time during endothelial cell culture, Liu et al. developed a system using ion-liquid-filled microchannels as variable resistors. Deformation of a PDMS membrane was used to transmit pressure changes from the cell culture channel, which were then converted into electrical signals. Under a shear stress of approximately 12.08 dyn·cm^{-2}, different levels of hydrostatic pressure ranging from 41.7 to 112.3 mmHg can be generated, effectively simulating the mechanical microenvironment experienced by vascular endothelial cells in vivo[163].

Gas

Metabolic processes directly depend on the supply of gases (e.g., oxygen), necessitating synchronized monitoring of gaseous parameters. Phosphorescence-based optical oxygen sensors are frequently used in in vitro cell culture platforms[164]. As shown in Fig. 10c, Izadifar et al. integrated oxygen-sensitive nanoparticles into a polycarbonate layer to enable real-time quantitative monitoring of oxygen concentration by tracking changes in near-infrared fluorescence signals. Under normal physiological conditions, the oxygen level in the gut-on-a-chip environment dropped from 21% to 5%, whereas treatment with oligomycin raised the O_2 concentration to 60%[17]. Schneider et al. integrated optical sensors and electrical stimulation electrodes into the chip. Using a near-infrared fluorescence lifetime-based oxygen sensor, they achieved detection of oxygen partial pressure changes as small as ≤1 hPa. During electrical stimulation, myocardial tissue exhibited enhanced metabolism and increased oxygen consumption, causing the oxygen partial pressure in the chip to drop from approximately 80 hPa to 60 hPa[45].

Electrochemical oxygen sensors are also commonly integrated into OoC systems for detecting gaseous components in the microenvironment. In liver-on-a-chip models, oxygen gradients are considered essential for reproducing the metabolic zonation found in liver microarchitecture. Moya et al. used inkjet printing to fabricate oxygen sensors and integrated them into an ultrathin porous cell culture membrane within a liver chip. The resulting dissolved oxygen (DO) sensor exhibited a LOD of 0.11 ± 0.02 mg/L and a sensitivity of approximately 28 nA·L/mg, enabling precise monitoring of hypoxic conditions where oxygen levels dropped below 2 mg/L due to hepatic metabolism[19]. Under hypoxic conditions, intestinal epithelial cells rapidly form barrier structures. As shown in Fig. 10d, with DO and ROS electrochemical sensors embedded, the intestinal barrier conditions under both hypoxic and normoxic conditions can be analyzed in real time. The DO and ROS sensors exhibited LOD of 0.67 mg/L and 1.7 μM, respectively, enabling coverage of oxygen levels during gut-on-a-chip development and capturing the initial ROS release triggered by hypoxia[165].

Temperature and pH

Maintaining stable and appropriate temperature and pH parameters is critical for ensuring cellular viability. Temperature is typically regulated directly by incubators,

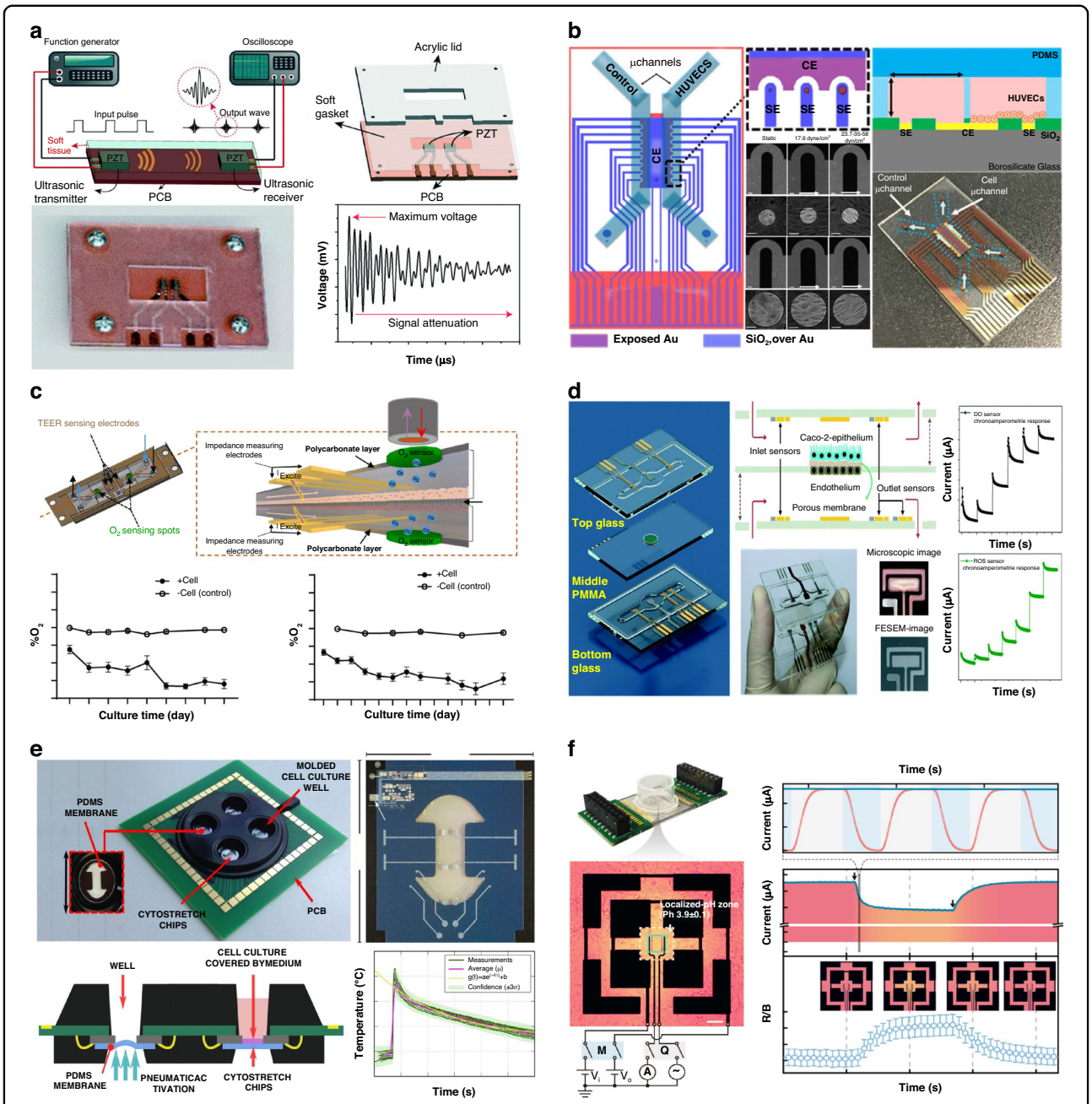

Fig. 10 Integrated sensing strategies for real-time monitoring of key physicochemical parameters in OoC microenvironments. Monitoring of mechanical conditions in the microenvironment: **a** Ultrasound-assisted OoC platform allows in situ investigation of ECM mechanical properties[154]; **b** Impedance sensors in microfluidics enabled real-time monitoring of endothelial response to shear stress[162]; Oxygen monitoring in culture environments can be achieved through the following approaches: **c** Autonomous hypoxic microenvironment generation and oxygen dynamics monitoring in OoC[17]; **d** Electrochemical sensing of DO and ROS enables continuous evaluation of barrier integrity and cellular stress in intestinal models[165]; In situ temperature and real-time pH monitoring: **e** Real-time temperature mapping of cellular processes using CMOS sensors[171]; **f** Graphene-based pH sensor enables high-precision regulation and real-time monitoring of cellular microenvironment[173];

yet discrepancies frequently exist between incubator settings and actual temperatures at tissue culture sites. For temperature sensing in cell culture, electrical methods primarily rely on commercial thermocouples[166] or thermistors[167]. However, when integrated into the culture environment, these sensors often introduce various sources of interference due to poor physical conformity with the system. Nonelectrical temperature sensing methods have also been reported, including liquid crystal displays[168], fluorescent polymer thermometers[169], and

Table 3 Comparative Analysis of Core Sensing Strategies

	Electrical Sensing	Mechanical Sensing	Optical Sensing
Detection Targets	Molecules Cells/Tissues Microenvironment	Cells/Tissues	Molecules Cells/Tissues Microenvironment
Measured Parameters	Electrophysiological Signals, Barrier Function Molecular Concentration	Tissue Deformation, Matrix Properties	Molecular Concentration, Cell Morphology Tissue Deformation Barrier Function;
Integration Difficulty	Medium ~ High	Medium ~ High	Low ~ High
Technology Maturity	High (Microelectrode) Medium (Biosensing)	Medium (Basic Sensors), Low (Novel Sensors).	High (Microscopy), Medium (Integrated Sensors)
Ref.	124–130,135–139,189,190	97,98,103,193–197	17,31,41,72,101–106,201,202,204–206

photoacoustic techniques[170]. Nevertheless, these approaches generally suffer from limited temperature resolution (~1 °C). In Fig. 10e, Ponte et al. developed a real-time CMOS temperature sensor that enables in situ monitoring of the full cell division cycle, with a temperature resolution of 0.2 °C[171]. Another team used silk-based materials as sensing and encapsulation layers, with nitrogen-doped carbon nanofibers serving as the active layer. As the temperature rises, the captured electrons gain energy and are released. Within the operating range of 35–63 °C, a linear response with a sensitivity of 1.75%/°C to temperature was achieved[172].

Chemical parameters constitute the immediate environment in which cells survive and carry out biochemical reactions. Among them, the pH value of the microenvironment can both influence and reflect the physiological state of cells. Figure 10f illustrates a system that integrated micro-electrolysis with graphene-based electronic pH sensing, enabling precise control of the microenvironmental pH (error < 0.1 pH units) along with excellent spatial and temporal resolution. This device modulated local pH through pulsed electrolysis and monitored changes in real time via a graphene field-effect transistor. It successfully regulated the motility of Bacillus subtilis and the calcium signaling and necrotic injury of cardiomyocytes[173]. Hande et al. utilized a floating-gate field-effect transistor to monitor pH changes in the culture region, while employing the extended portion of the floating gate as microelectrodes to record cortical neuronal electrical activity. Upon introducing 50 μM mucoricin to induce epilepsy-like activity in the cultured cells, they simultaneously monitored electrical signals and pH fluctuations, providing insights into the relationship between disease phenotypes and cellular viability[174].

Challenges in microenvironmental monitoring

Conventional microenvironmental monitoring methods provide averaged readings of the microenvironment and fail to capture the spatial gradients essential to cellular functions. For instance, thick tissues such as brain organoids often develop nutrient gradients due to diffusion limitations, making it difficult for traditional sensors to reveal internal metabolic heterogeneity. Despite the complex fabrication process, sensor arrays with high density can simultaneously monitor metabolite and ion concentrations at hundreds of sites, enabling real-time mapping of the spatial topology of microenvironmental parameters[175]. Therefore, for application scenarios requiring high spatial resolution, the manufacturing of devices can be facilitated by the latest nanofabrication technologie[176].

On-chip sensing elements

Sensing elements serve as the physical carriers for in situ monitoring, requiring fulfillment of core requirements including miniaturization, biocompatibility, and high sensitivity. Based on their sensing mechanism, these elements can be categorized into electrical, mechanical, and optical methods, all demonstrating significant potential for implementing in situ sensing within OoC systems. Table 3 compares the three primary sensing strategies used in OoC.

Electrical sensing technologies exhibit high maturity. In cardiac and neural chips based on well-established microfabrication techniques, microelectrode arrays have been widely implemented. The main challenge at moderate to high integration levels lies in fabricating high-density, high SNR microelectrodes within the limited chip area while maintaining long-term stable electrical interfaces.

Mechanical sensing is indispensable for monitoring tissue mechanical functions. The basic sensing technologies have moderate maturity, but the main challenge lies in noninvasively embedding sensors into soft matrices and accurately detecting subtle mechanical signals.

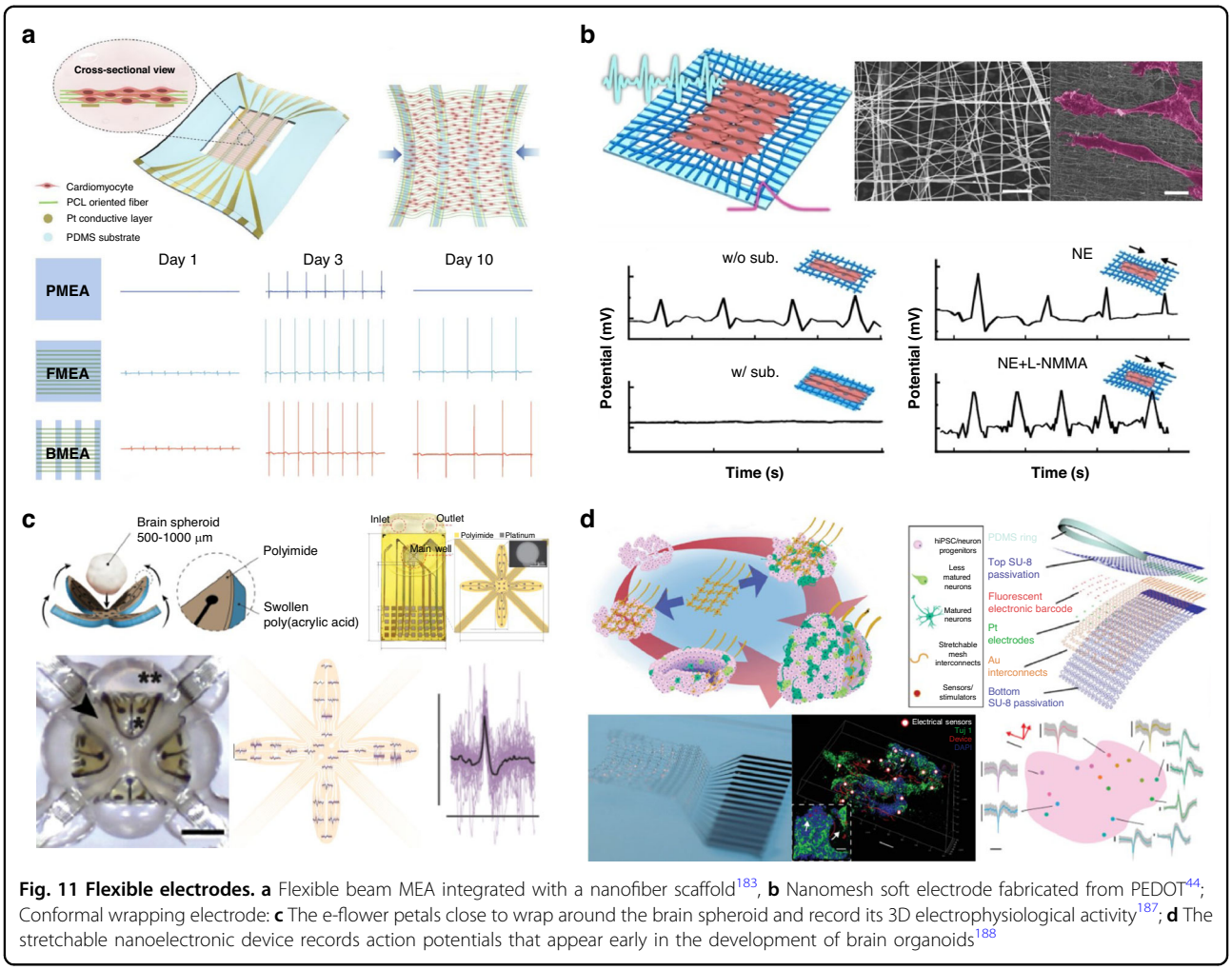

Fig. 11 Flexible electrodes. a Flexible beam MEA integrated with a nanofiber scaffold[183], **b** Nanomesh soft electrode fabricated from PEDOT[44]; Conformal wrapping electrode: **c** The e-flower petals close to wrap around the brain spheroid and record its 3D electrophysiological activity[187]; **d** The stretchable nanoelectronic device records action potentials that appear early in the development of brain organoids[188]

In optical sensing, the use of external microscopes for observation represents the most basic form of integration and remains the most mature approach. In contrast, on-chip integration of optical components such as waveguides and light sources involves a much higher level of integration complexity.

Electrical elements

Electrodes are the most commonly used elements for in situ sensing in OoC systems. They can be directly embedded or attached to cell culture chambers to monitor the electrophysiological activity of tissues or concentration changes of specific molecules in real time. Depending on the target being detected, electrodes can be divided into electrophysiological electrodes and electrochemical electrodes.

Electrophysiological electrodes

Electrophysiological electrodes are primarily used to monitor the electrophysiological activity of cells and tissues, especially playing a crucial role in organs such as the heart and brain. Electrophysiological electrodes can be classified into traditional electrodes and flexible electrodes based on materials, structure, and usage requirements. Traditional electrodes, typically made of noble metals like Au and Pt[177–179], are deposited on rigid substrates, e.g. silicon or glass[180–182]. Compared to traditional electrodes, flexible electrodes have better elasticity and adaptability, allowing compliance to biological tissues and be used for long-term monitoring of tissues or organoids. As shown in Fig. 11a, the flexible beam MEA integrated with a nanofiber scaffold enables the in vitro cultivation of more mature cardiomyocytes while allowing real-time monitoring of electrophysiological signals[183]. In Fig. 11b, a nanomesh soft electrode fabricated from PEDOT demonstrates excellent mechanical flexibility, electrical conductivity, and cellular biocompatibility[44]. Cardiomyocytes cultured on this soft nanomesh exhibit spontaneous and rhythmic contraction–relaxation behavior, enabling in situ and real-time monitoring of both biomolecular release and electrophysiological activity in dynamically beating cells. Therefore, in order to better match the

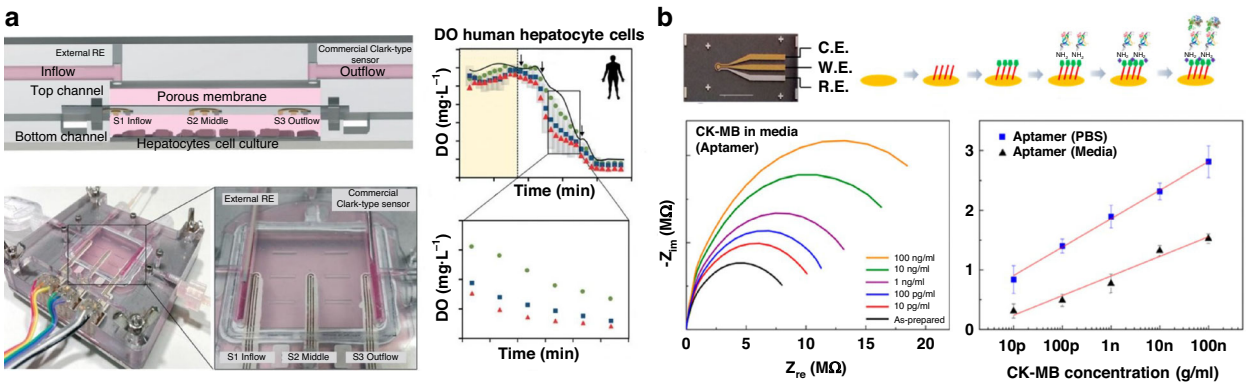

Fig. 12 Electrochemical electrodes. a Basic electrodes to monitor oxygen in liver-on-a-chip[19]; **b** Functionalized electrodes to monitor trace CK-MB secreted by cardiac organoids[189]

mechanical properties of in vitro tissues, flexible electrodes are expected to play an increasingly important role in future electrophysiological monitoring.

With the continuous advancement of materials science and micro/nano fabrication technologies, electrode structures have also undergone a transition from 2D to 3D structures. The main reason for this transition lies in that it better meets the monitoring needs of organoids. The 3D electrode structure can more accurately conform to the complex architecture of organoids, thereby improving the precision and reliability[184,185].

To achieve real-time in situ sensing in vitro tissue models, sensors with mechanical properties matched to those of native tissue can reduce local stress concentrations, conform to dynamic tissue movements, preserve cellular physiological functions, and minimize interfacial interference[186]. As shown in Fig. 11c, in the brain-on-chip model, Martinelli et al. designed an intuitive flexible MEA named e-Flower. The e-Flower consisted of a layer of flower-shaped polyimide film, which was divided into four flat petals. Each petal contained eight Pt microelectrodes and was coated on the back with a layer of grafted polyacrylic acid hydrogel. The swelling properties of the hydrogel drive the e-Flower petals to close and wrap around the brain spheroids, thereby recording their 3D electrophysiological activity[187]. Floch et al. designed a stretchable nanoelectronic device that perfectly matches the mechanical properties of brain organoids (Fig. 11d). This device did not interfere with the development of brain organ tissue, while being adaptable to the volume and morphological changes during the development process of brain organoids. It also maintained long-term stable contact with neurons within the brain organoid tissue. Through seamless, non-invasive coupling between the electrodes and neurons, stable and continuous recordings for up to six months were achieved. This technology successfully captured the single-cell action potentials that appeared early in brain organoid development, providing valuable application prospects for research on brain organoids at the early developmental stage[188].

Electrochemical electrodes

Electrochemical electrodes in OoC systems are primarily used for biochemical monitoring of cells and tissues. Based on surface modification strategies, electrochemical electrodes can be classified into two main categories: basic and functionalized types. Basic electrodes (such as glassy carbon, gold, and platinum microelectrodes) directly leverage the intrinsic electrocatalytic properties of the electrode materials to detect endogenous electroactive species through redox reactions, without requiring complex surface engineering. Basic electrodes are commonly used in OoC systems for real-time monitoring of simple molecules such as oxygen and H_2O_2. For example, in liver-on-a-chip systems for oxygen monitoring, Moya et al. fabricated gold/silver-based electrodes using inkjet printing, leveraging the intrinsic electrocatalytic activity of the materials to monitor oxygen concentration gradients[19]. In a study on vascular-on-a-chip platforms, electrochemical electrodes were developed by combining the conductive polymer PEDOT with carbon nanotubes. PEDOT enhanced the electrocatalytic response to NO and H_2O_2 (representative of ROS), while the carbon nanotubes improved the conductivity and mechanical flexibility of the electrodes[57]. Their advantages include rapid response and ease of fabrication. However, their selectivity is limited due to interference from the coexistence of multiple electroactive substances in the biological microenvironment Fig. 12.

Functionalized electrodes impart molecular specificity through surface modification with biorecognition molecules. Among these, enzyme electrodes (e.g., glucose oxidase-modified electrodes) utilize enzymatic reactions to

convert non-electrochemically active substrates (e.g., glucose, lactic acid) into detectable electrochemically active products, and have been widely applied in metabolic kinetic studies of liver-on-a-chip[16] and muscle-on-a-chip systems[56]. Aptamer sensors, on the other hand, rely on high-affinity binding between antigen-antibody pairs or aptamer-target complexes to directly induce changes in interfacial impedance or current signals, enabling ultrasensitive detection of low-abundance biomarkers such as cytokines and exosomes. To monitor trace creatine kinase MB (CK-MB) secreted by cardiac organoids, Shin et al. immobilized CK-MB-specific aptamers on gold electrodes and detected changes in charge transfer resistance (R_{ct}) induced by aptamer-target binding using EIS. The sensor achieved a LOD of 2.4 pg/mL[189]. For in vitro hepatotoxicity assessment, an electrochemical microsensor for alanine aminotransferase (ALT) activity was developed. This sensor employed glutamate oxidase immobilized via drop-casting on screen-printed electrodes, enabling evaluation of ALT activity by detecting changes in glutamate concentration[190]. Despite their exceptional selectivity, such electrodes face challenges including instability of modification layers and interference from complex sample matrices.

For monitoring multiple biomarkers, two or more electrochemical electrodes can be integrated to independently detect targets. In a study by Weltin et al., two electrochemical electrodes were integrated to enable simultaneous monitoring of lactate and oxygen. Lactate detection was achieved using a lactate oxidase-modified platinum electrode, while an unmodified platinum electrode facilitated the direct reduction reaction of oxygen. This sensor platform leveraged both the lactate oxidase-modified electrode and platinum-based oxygen electrode to precisely quantify lactate production rate (5.1 μM/h), confirming the absence of hypoxia in the cultured microenvironment[191].

On-chip strategies and challenges

Electrical sensing elements are the most direct means of achieving high spatiotemporal resolution and in situ monitoring in OoC, with their performance highly dependent on electrode integration strategies. Successful integration must not only ensure electrode stability but also minimize interference with the microphysiological environment. Integration of electrical elements primarily relies on established micro- and nanofabrication techniques. Processes such as photolithography, metal deposition, and lift-off on glass, silicon, or flexible polymer substrates enable the one-step fabrication of high-precision microelectrode arrays and interconnects[177–179]. For flexible chips, transfer printing is often employed to move entire circuits onto elastomers such as PDMS[36,44,192]. In addition, additive manufacturing methods such as inkjet printing provide versatile approaches for the rapid fabrication of customized electrodes[19]. Integrated electrical elements must also ensure long-term stability in wet environments, while robust wiring encapsulation and interface techniques are required for efficient connection with external readout circuits.

Mechanical elements

Mechanical sensing elements monitor biomechanical activities via deformation-signal transduction mechanisms and can be classified into thin-film and microstructured sensors. Their key advantage lies in directly capturing dynamic processes such as tissue contraction and deformation, making them especially suitable for organ models with frequent mechanical activity and pronounced deformation (e.g., beating heart, breathing lung tissue). Structural innovations in these sensors significantly enhance critical performance metrics such as sensitivity, responsiveness, and integration capability.

Thin-film sensors

Thin-film sensors capture mechanical signals through planar functional layers. Their core innovation lies in the integration of flexible substrates with micro/ nanomaterials, granting exceptional flexibility and stretchability. This allows them to conform closely to the dynamic deformation of biological tissues or organ models. Such structural design minimizes interference from rigid devices, enabling more natural mechanical coupling. As shown in Fig. 13a, Chen et al. proposed a flexible strain sensor based on a triboelectric nanogenerator with a bridge structure. During an 11-day continuous monitoring and drug treatment test of myocardial tissue, the sensor exhibited good SNR and stability, capable of recording the dynamic changes caused by myocardial cell contraction. Its strain LOD is 0.025%[98]. Adadi et al. developed an electrospun fiber scaffold based on PVDF, which not only supports cell growth and adhesion but also has mechanical responsiveness due to the inherent properties of PVDF. This allows it to directly monitor tissue contraction activity, simplifying the manufacturing process and reducing cost[97].

Building on the thin-film structure, integrating functional materials further enables strain monitoring in engineered tissues cultured in vitro. Li et al. designed a novel heart-on-a-chip system using an integrated reduced graphene oxide mixed anisotropic colored film for cardiac sensing and evaluation. This mixed anisotropic film is based on the opposing adhesive properties of polyethylene glycol diacrylate (PEGDA) and methacrylated gelatin (GelMA). When myocardial cells beat, their elongation and contraction stretch the PEGDA structure, resulting in color changes, thus enabling the transition from microscopic mechanical to macroscopic optical changes[103]. To

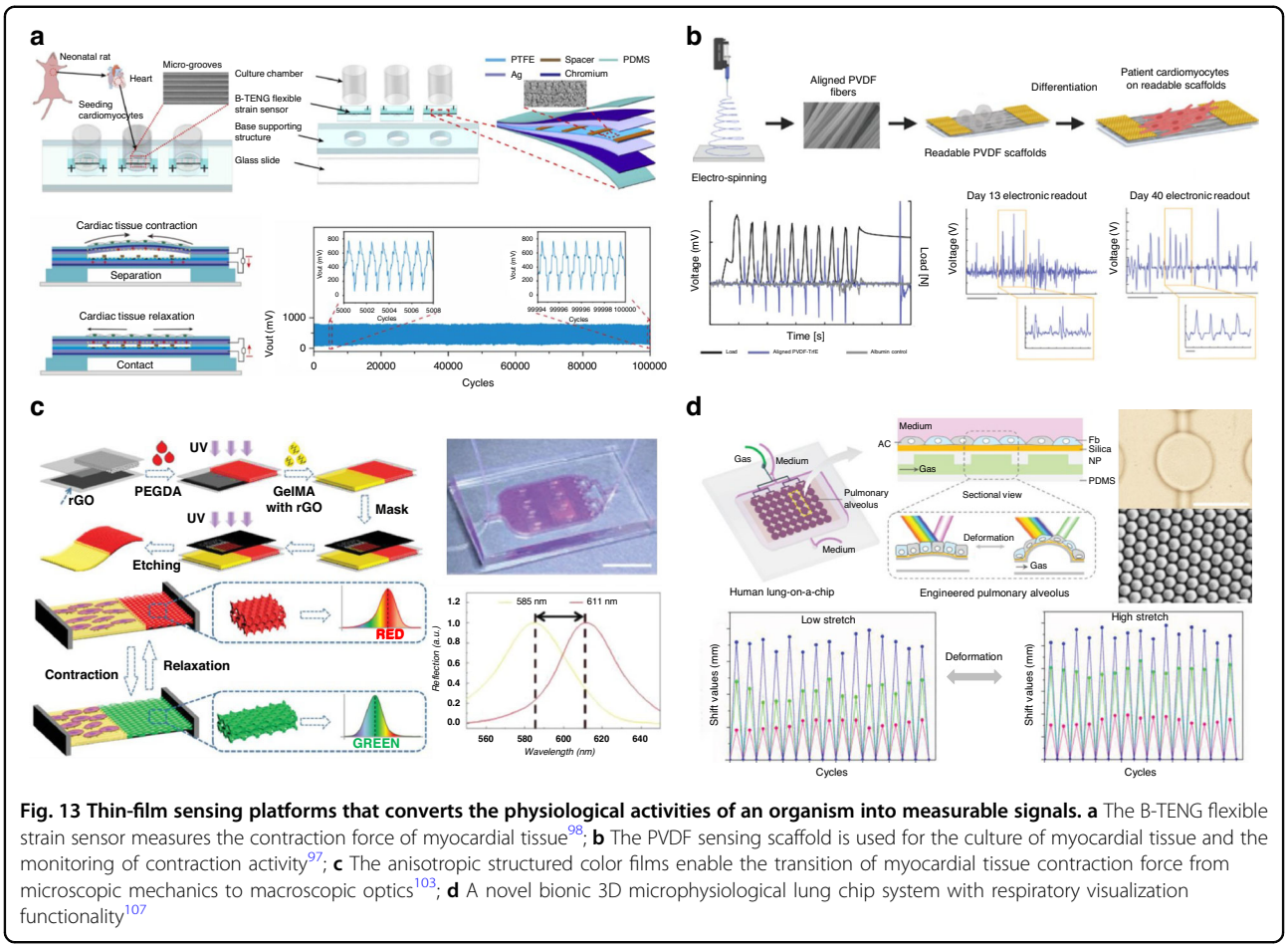

Fig. 13 Thin-film sensing platforms that converts the physiological activities of an organism into measurable signals. a The B-TENG flexible strain sensor measures the contraction force of myocardial tissue[98]; **b** The PVDF sensing scaffold is used for the culture of myocardial tissue and the monitoring of contraction activity[97]; **c** The anisotropic structured color films enable the transition of myocardial tissue contraction force from microscopic mechanics to macroscopic optics[103]; **d** A novel bionic 3D microphysiological lung chip system with respiratory visualization functionality[107]

monitor the stress distribution during the breathing process of a lung-on-a-chip, Zhu et al. coated structural color materials onto the surface of a PDMS membrane, developing a novel biomimetic 3D microphysiological lung-on-a-chip system with breathing visualization functionality. This system is used to simulate alveolar arrays at a physiological scale. The periodic airflow induces cyclic deformation, similar to the expansion and contraction of alveoli during rhythmic breathing. The deformation, accompanied by synchronous changes in structural color, enables real-time monitoring of the culture process[107].

Microstructured sensors

Microstructured sensors detect tissue forces through designed microscale 3D mechanical elements (e.g., beams, pillars). In contrast to thin-film sensors that primarily conform to surfaces, their 3D architectures generated more pronounced deformations and exhibit enhanced mechanical specificity. This substantially enhances sensitivity and facilitates the integration of mechanical actuation with sensing, as well as parallel multi-parameter measurements.

The core innovation of cantilevers and microbeams lies in their fixed-end structural design. When a small force is applied by the tissue to the free end, the resulting deformation at the tip is significantly amplified due to the lever principle, effectively functioning as a precise mechanical amplifier. As shown in Fig. 14a, Kim et al. proposed a cantilever device integrated with a crack-based sensor encapsulated in PDMS, By leveraging the sharp resistance change caused by crack propagation under microstrain and combining it with deformation amplification from cantilever structures, highly sensitive measurement of contractile forces can be achieved[28]. Sun et al. incorporated a monocrystalline silicon strain sensor into an SU-8 cantilever to enhance sensitivity for measuring cardiomyocyte contraction. Experimental results demonstrated a minimum detectable force of 0.02 μN, with sensitivity nearly 17 times higher than conventional metal strain gauges[193]. Figure 14c illustrates a FBG integrated microbeam. Myocardial contraction deforms the microbeam, inducing a wavelength shift in the FBG. With a sensitivity of up to 117.5 pm/mN, this system enabled precise detection of subtle contractile forces at the micronewton scale[102].

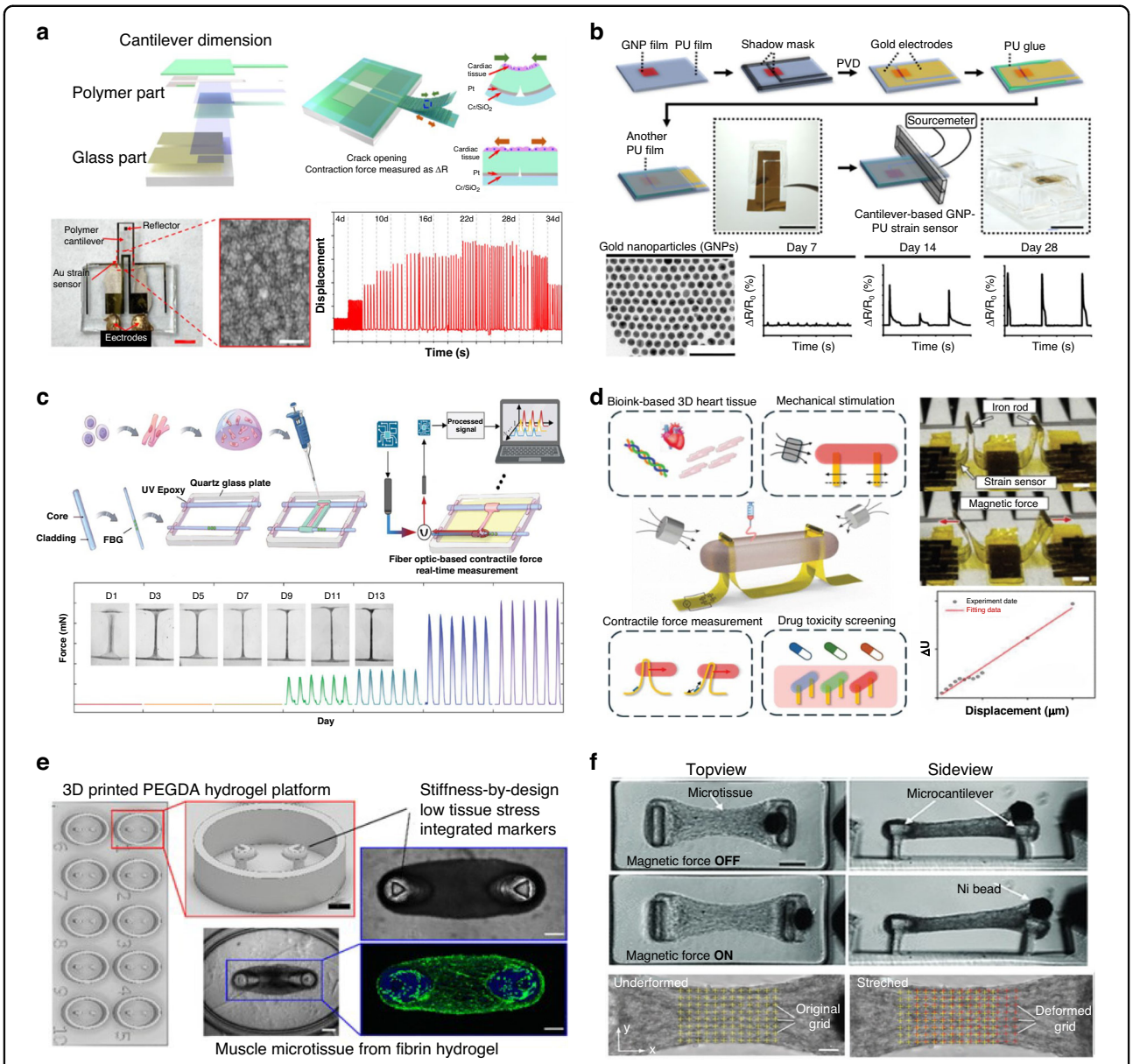

Fig. 14 Strain sensor sensitivity can be enhanced through microstructural designs such as cantilevers. a Cantilever device integrated with a crack-based sensor for contractile force measurement[28], **b** Self-healing hydrogel combined with a cantilevered GNP-PU strain sensor for monitoring contraction behavior of cardiac spheroids[195]; Micropillars: **c** FBG-based optical fiber sensor for measuring hEHT contractile force[102], **d** Origami-inspired sensor for measuring contractile force in 3D cardiac tissue[196]; Microbeams: **e** Stereolithographically 3D-printed multiplexed platform with tunable mechanical properties[194], **f** Magnetically actuated micropillars for 3D microtissue arrays[197]

Combined with 3D printing technology, micropillar structures enable the construction of complex, customizable physiological microenvironments and support high-throughput analysis. As shown in Fig. 14f, Christensene et al. employed photocurable 3D printing to fabricate a micropillar array platform using PEGDA with tunable stiffness. By designing regions with distinct mechanical properties and incorporating optical markers, they enabled parallel and quantitative monitoring of multiple muscle bundle contractions[194].

3D microstructures also provide a versatile platform for multifunctional integration. Wu et al. employed a self-healing chitosan hydrogel as a carrier for cardiac spheroids and directly integrated it with a cantilever-type GNP-PU strain sensor (Fig. 14b). The hydrogel not only mimicked the physiological environment but also served as a compliant mechanical bridge, transmitting cellular motion to the rigid cantilever sensor. This design effectively addressed the challenge of mechanical coupling between rigid sensors and soft 3D tissues, enabling in situ

and real-time monitoring of spheroid contraction dynamics[195]. In Fig. 14d, the creases of a folded polyimide substrate function as microbeams. Magnetic microrods and gold strain sensors were integrated at the crease and fold base, enabling a single structure to simultaneously deliver magnetically driven mechanical stimulation and passively monitored tissue contraction forces with high sensitivity[196]. Figure 14f illustrates a magnetically actuated micropillar system in which the micropillars function both as anchorage points for tissue attachment and as stimulatory elements manipulated by an external magnetic field. This platform facilitates in situ, noninvasive quantification of pillar deflections induced by spontaneous tissue contractions, while concurrently applying dynamic and controllable mechanical stimuli. Real-time monitoring of the tissue's mechanical responses enables the establishment of a closed-loop "stimulus-response" analytical system[197].

On-chip strategies and challenges

The integration of mechanical sensing components depends on the sensor type, chosen materials, and compatibility with biological tissues. Thin-film sensors are typically fabricated directly onto the chip substrate through processes such as spin coating or vapor deposition, forming a monolithic "sensor–substrate" structure[98,103]. For three-dimensional structures such as micropillars and microbeams, soft lithography is often used to mold them together with the microfluidic chamber in a single step[194,197], or they can be integrated into designated positions within the chip through precision assembly[28,196]. The primary goal of mechanical integration is to address mechanical mismatch, which is usually mitigated by selecting low-modulus materials or employing structural designs that buffer and transmit stress. This ensures that the natural physiological activities of biological tissues remain undisturbed while enabling high-fidelity transmission of mechanical signals.

Optical elements

Optical sensing technologies enable non-invasive, in situ analysis of microphysiological activities by harnessing fundamental interactions between light-matter interactions, consisting of photon absorption, emission, reflection and refraction. These interactions can be systematically leveraged to construct on-chip optical sensing elements, providing multiscale insights into processes ranging from molecular metabolism to cellular interactions in in vitro tissue models.

Luminescent and absorptometric sensing

The physical basis of luminescent sensing lies in the photon emission during electronic energy level transitions of molecules. Target analytes alter the emission intensity or efficiency by affecting the energy transfer or transition processes of luminescent molecules. In OoC systems, widely used immunofluorescence techniques are a common form of luminescence-based sensing. However, they typically require external excitation light sources and are limited to endpoint detection. In contrast, optical biosensors based on bioluminescence imaging enable continuous, noninvasive, and in situ imaging of cells, tissues, or miniature organs[198,199]. By pairing NanoLuc luciferase with its substrate Furimazine and employing confocal microscopy, single-cell bioluminescence imaging on-chip can be achieved. Compared to conventional fluorescence detection, the inherently low background of bioluminescent signals significantly enhances the SNR of on-chip imaging[200].

Luminescence-based sensors can be constructed by embedding luminescent probes directly into the cell culture regions of the chip. Changes in the concentration of target analytes lead to measurable variations in fluorescence intensity[31,201,202]. For instance, ruthenium-phenanthroline-based phosphorescence dye loaded in microbeads (CPO_x-50-RuP) have been integrated into chips to monitor hepatic oxygen consumption in real time, allowing the study of different hepatocyte responses to acetaminophen[82]. Additionally, when constructing hypoxic microenvironments, PtOEP films are used as light-emitting sensors, where fluorescence intensity varies with oxygen concentration, enabling real-time assessment of hypoxic conditions[41]. Directly embedding probes into the tissue enables more sensitive detection of target analyte concentrations, as shown in Fig. 15a, Poon's group embedded tetrapodal zinc oxide (t-ZnO) microparticles into neural tissue using 3D printing. Dopamine (DA) induces fluorescence quenching of t-ZnO, enabling highly sensitive (LOD as low as 0.137 μM) and highly selective detection of DA by monitoring changes in fluorescence intensity[203].

Absorption-based sensing contrasts with luminescence-based methods, where analyte concentration modifies absorbance. For instance, incorporating absorptive indicators (e.g., phenol red) directly into culture medium enables continuous pH monitoring through transmission intensity measurements, achieved by positioning optical sources and photodetectors adjacent to transparent chip substrates[17,204–206]. In the liver-on-a-chip device developed by Farooqi for drug toxicity monitoring, a glass microfluidic chip was embedded with ITO electrodes and an optical pH sensor. Combined with a 3D-printed portable microscope, the system enabled dynamic monitoring of both the TEER of HepG2 liver cells and the pH of the culture medium. Upon doxorubicin-induced toxicity, it was observed that higher drug concentrations led to more pronounced decreases in TEER and greater reductions in pH[205].

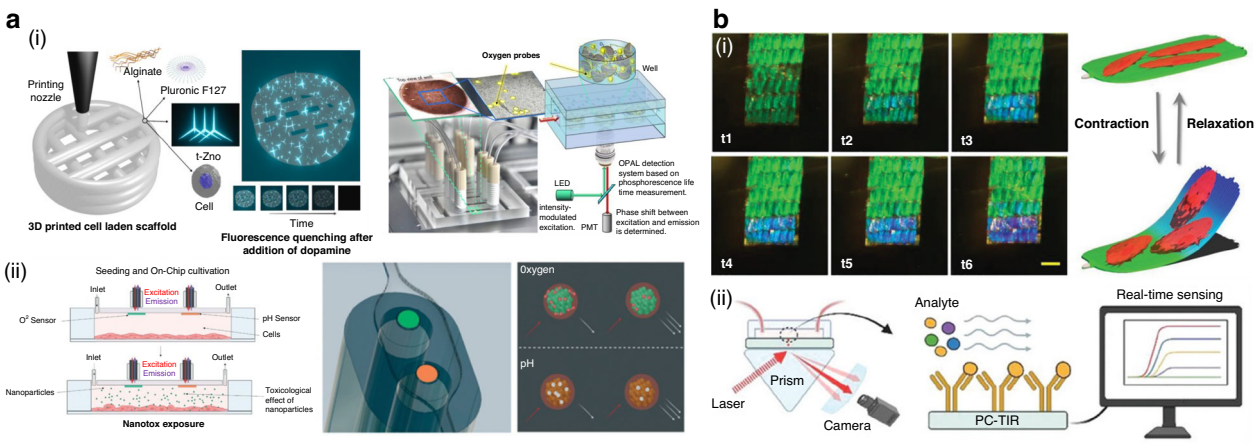

Fig. 15 Optical sensing modalities for monitoring biochemical and biophysical parameters. a Luminescence-based sensing for detecting dopamine and oxygen consumption[203] (i) and absorbance-based sensing for measuring oxygen concentration and pH levels[208](ii); **b** Reflective sensing for detect cardiomyocyte contractions[106](i), and refractive index changes for monitoring biomarkers[72] (ii)

Optical fibers enable deep-tissue or localized signal acquisition by transmitting excitation light and collecting emitted light[75]. For instance, Jennifer et al. combined optical fibers with oxygen-sensitive nanoparticles to construct an oxygen sensor within a gut-on-a-chip, enabling quantitative detection of oxygen levels in anaerobic environments[207]. Similarly, fluorescence signals transmitted via optical fibers have been used in vascular chips to quantify metabolic disturbances induced by nanoparticles (Fig. 15a)[208]. Beyond microenvironmental monitoring, the research team led by Koppes developed a non-invasive, fiber-optic luminescence sensing platform that delivers excitation light (430 nm) and collects emitted fluorescence (520 nm) through optical fibers, enabling real-time monitoring of epithelial/endothelial barrier integrity within OoC systems[144].

Reflective and refractive sensing

In OoC optical sensing, the propagation behavior of light was utilized to analyze tissue structures and molecular interactions. FBG can be directly embedded within tissue culture regions as sensitive strain sensors, detecting myocardial tissue contractions by tracking shifts in their characteristic reflection peaks and transmission dips[102]. Anisotropic structural color materials represented another paradigm for constructing sensing elements via light reflection. By integrating these materials as cell culture substrates within microphysiological systems, cells grow and function directly on the sensing surface. In one study, cardiomyocytes were cultured on the surface of butterfly wings. The cells aligned and began to beat spontaneously, which induced deformation of the wing substrate, altering the angle of light incidence and causing a blue shift in the reflection spectrum, thereby converting mechanical signals into optical signals[106]. Structural color modulation was also achieved using inverse opal structures, which provided stable structural coloration. The sensing mechanism similarly relied on cardiomyocyte beating to bend the hydrogel, thereby changing the light incidence angle, with the wavelength shift of the reflection spectrum positively correlated with the bending angle[105].

When light passes through an interface, its path bends due to a change in propagation speed. By leveraging the alteration of local refractive index caused by biomolecular interactions, molecular detection can be achieved in OoC systems. Wu et al. employed gold nanoslit arrays to generate asymmetric Fano resonances. When the target molecule MMP-9 bound to the sensor surface, it induced a local refractive index change, leading to shifts in both the resonance wavelength and intensity[74]. Quantitative detection is accomplished by monitoring variations in the transmission spectrum. Similarly, a localized surface plasmon resonance sensor based on gold nanorod arrays has been developed. When insulin bound to antibodies immobilized on the sensor surface, the resulting change in refractive index causes a redshift in the resonance wavelength, enabling quantitative analysis by tracking spectral shifts[73]. Yang et al. utilized a PC-TIR interface to form an open optical microcavity that is highly sensitive to surface molecular binding. When liver-secreted biomarkers such as albumin or GST-α bind to antibodies immobilized on the sensor surface, the resonance angle shifts, which can be monitored via reflected light imaging[72].

The integration of electrical, mechanical, and optical sensing elements is pivotal for achieving multimodal synchronous monitoring, representing the evolutionary trajectory for future OoC sensing systems.

On-chip strategies and challenges

The noninvasive nature of optical sensing makes it an ideal choice for OoC. The highest level of integration embeds optical functionalities directly within the chip, for instance by incorporating fluorescence-sensitive particles into the PDMS matrix[41,82] or by fabricating integrated optical waveguides on the substrate[72,74]. A more common approach is in-chip integration, where miniature optical fibers are inserted near microchannels to deliver and collect optical signals[144,207,208]. Many systems also adopt beside-chip integration, which leverages the transparency of the device for observation using external microscopes[17,206]. Future development is expected to focus on truly on-chip optical microsystems, integrating micro-LEDs, photodetectors, and filters into a single device to ultimately eliminate reliance on bulky external optical equipment.

Conclusions and perspectives

OoC replicate the physiological microenvironment of human organs, enabling more accurate reproduction of organ structure and function, and thus offering a research platform that better reflects in vivo conditions. The integration of on-chip sensors is driving a fundamental transformation in organ-on-a-chip technology, shifting it from "static biomimicry" to "dynamic monitoring". First, it overcomes the temporal limitations of traditional endpoint assays by converting single static snapshots into "continuous imaging" of biological processes, thereby capturing critical transient events such as biomarker secretion and the evolution of arrhythmias. Second, the integration of multiple sensors enables multimodal sensing, by simultaneously tracking electrophysiological, mechanical, and biochemical parameters, which reveals interactions across different functional perspectives and establishes a factual basis for understanding biological response mechanisms.

This review also identifies monitoring targets at three different levels: biomolecules, cellular and tissue behaviors, and microenvironmental parameters. The commonly used sensing elements for these targets are further categorized according to their sensing principles, with focus on the innovations that enable continuous, real-time, and in situ monitoring. These technological advances provide essential support for comprehensive and in-depth studies of OoC.

However, although OoC platforms have facilitated the development of various pathogen infection models, some models have not yet achieved on-chip monitoring[209]. For example, in human alveolar chips infected with SARS-CoV-2, it is still necessary to collect cells or culture medium from the chip for offline analysis[210]. Similarly, when using liver chips to study hepatitis B virus infection, the detection of cytokines and quantification of viral replication levels still rely on offline methods such as ELISA or nucleic acid amplification[211]. In the future, integrating electrochemical sensors onto chips may enable real-time monitoring of concentration changes in relevant signaling molecules.

With the advancing of on-chip modeling, OoC systems are expected to simulate increasingly complex physiological environments in vitro. These advancements range from recreating multi-organs interactions to constructing dynamic disease models. These emerging models introduce a wider range of sensing targets, including metabolic signal transduction at organ interfaces, interactions between the extracellular matrix and immune cells, and gene expression changes induced by mechanical stress. Detecting such events presents new challenges for sensing technologies, such as capturing weak signals in high-noise environments, resolving subcellular activities with high spatial resolution, and achieving dynamic response and tracking of biological activities. To address these challenges, future OoC will bring up the need for sensing technologies that deeply integrate both multidimension and multiscale strategies. Such integration can provide more comprehensive physiological data from the tissues/organs on the chip and even establish a complete causal chain from molecular events to organ functions. Aided by the artificial intelligent, such OoC system will enable the development of truly intelligent OoC, offering new screening tools for drug development and personalized therapy.

Acknowledgements

This study was supported by the National Key Research and Development Program of China (2022YFB4600600).

Author contributions

S.L. and C.X. contribute equally to the article; Conceptualization, S.C., Z.D., and D.S.; Investigation, F.X., H.J., and Y.J.; Original draft, S.L. and C.X.; Review and editing, H.C. and S.C.

Conflict of interest

The authors declare no competing interests.

Received: 29 August 2025 Revised: 1 November 2025 Accepted: 18 November 2025
Published online: 13 February 2026

References

1. Leung, C. M. et al. A guide to the organ-on-a-chip. *Nat. Rev. Methods Prim.* **2**, 33 (2022).
2. Vunjak-Novakovic, G., Ronaldson-Bouchard, K. & Radisic, M. Organs-on-a-chip models for biological research. *Cell* **184**, 4597–4611 (2021).
3. Hosokawa, K. et al. Cell-free mRNA translation in a microbiochemical reactor. *1997 International Symposium on Micromechanics and Human Science (Cat. No.97TH8311)*, 91-95 (1997).
4. Hosokawa, K. et al. Microbiochemical reactors for enzymatic reactions including cell-free mRNA translation. *J. Micromechatron.* **1**, 85–98 (2000).
5. Huh, D. et al. Reconstituting organ-level lung functions on a chip. *Science* **328**, 1662–1668 (2010).

6. Sackmann, E. K., Fulton, A. L. & Beebe, D. J. The present and future role of microfluidics in biomedical research. *Nature* **507**, 181–189 (2014).
7. Ziółkowska, K., Kwapiszewski, R. & Brzózka, Z. Microfluidic devices as tools for mimicking the in vivo environment. *N. J. Chem.* **35**, 979–990 (2011).
8. Wang, Y. et al. Emerging trends in organ-on-a-chip systems for drug screening. *Acta Pharm. Sin. B* **13**, 2483–2509 (2023).
9. Tejavibulya, N. & Sia, S. K. Personalized disease models on a chip. *Cell Syst.* **3**, 416–418 (2016).
10. Huang, Y., Liu, T., Huang, Q. & Wang, Y. From organ-on-a-chip to human-on-a-chip: a review of research progress and latest applications. *ACS Sens* **9**, 3466–3488 (2024).
11. Zhang, Y. S. & Khademhosseini, A. Seeking the right context for evaluating nanomedicine: from tissue models in petri dishes to microfluidic organs-on-a-chip. *Nanomedicine* **10**, 685–688 (2015).
12. Hadavi, D., Tosheva, I., Siegel, T. P., Cuypers, E. & Honing, M. Technological advances for analyzing the content of organ-on-a-chip by mass spectrometry. *Front. Bioeng. Biotechnol.* **11**, https://doi.org/10.3389/fbioe.2023.1197760 (2023).
13. Kasendra, M. et al. Development of a primary human Small Intestine-on-a-Chip using biopsy-derived organoids. *Sci. Rep.* **8**, 2871 (2018).
14. Beussman, K. M. et al. Micropost arrays for measuring stem cell-derived cardiomyocyte contractility. *Methods* **94**, 43–50 (2016).
15. Zheng, Q. et al. Dynamic real-time imaging of living cell traction force by piezo-phototronic light nano-antenna array. *Sci. Adv.* **7**, eabe7738 (2021).
16. Bavli, D. et al. Real-time monitoring of metabolic function in liver-on-chip microdevices tracks the dynamics of mitochondrial dysfunction. *Proc. Natl. Acad. Sci. USA* **113**, E2231–E2240 (2016).
17. Izadifar, Z. et al. Organ chips with integrated multifunctional sensors enable continuous metabolic monitoring at controlled oxygen levels. *Biosens. Bioelectron.* **265**, 116683 (2024).
18. Meghani, N., Kim, K. H., Kim, S. H., Lee, S. H. & Choi, K. H. Evaluation and live monitoring of pH-responsive HSA-ZnO nanoparticles using a lung-on-a-chip model. *Arch. Pharmacal Res.* **43**, 503–513 (2020).
19. Moya, A. et al. Online oxygen monitoring using integrated inkjet-printed sensors in a liver-on-a-chip system. *Lab Chip* **18**, 2023–2035 (2018).
20. Ferrell, N. et al. A microfluidic bioreactor with integrated transepithelial electrical resistance (TEER) measurement electrodes for evaluation of renal epithelial cells. *Biotechnol. Bioeng.* **107**, 707–716 (2010).
21. Lind, J. U. et al. Instrumented cardiac microphysiological devices via multimaterial three-dimensional printing. *Nat. Mater.* **16**, 303–308 (2017).
22. Zhang, Y. S. et al. Multisensor-integrated organs-on-chips platform for automated and continual in situ monitoring of organoid behaviors. *Proc. Natl. Acad. Sci. USA* **114**, E2293–E2302 (2017).
23. Schocken, D. et al. Comparative analysis of media effects on human induced pluripotent stem cell-derived cardiomyocytes in proarrhythmia risk assessment. *J. Pharmacol. Toxicol. Methods* **90**, 39–47 (2018).
24. Asakura, K. et al. Improvement of acquisition and analysis methods in multi-electrode array experiments with iPS cell-derived cardiomyocytes. *J. Pharmacol. Toxicol. Methods* **75**, 17–26 (2015).
25. Schmidt, S. et al. Novel high-dense microelectrode array based multimodal bioelectronic monitoring system for cardiac arrhythmia re-entry analysis. *Biosens. Bioelectron.* **252**, 116120 (2024).
26. Kanade, P. P. et al. MEA-integrated cantilever platform for comparison of real-time change in electrophysiology and contractility of cardiomyocytes to drugs. *Biosens. Bioelectron.* **216**, 114675 (2022).
27. Lin, Z. C. et al. Accurate nanoelectrode recording of human pluripotent stem cell-derived cardiomyocytes for assaying drugs and modeling disease. *Microsyst. Nanoeng.* **3**, 16080 (2017).
28. Kim, D.-S. et al. Highly durable crack sensor integrated with silicone rubber cantilever for measuring cardiac contractility. *Nat. Comm.* **11**, 535 (2020).
29. Ou, L. et al. Real-time wireless sensing of cardiomyocyte contractility by integrating magnetic microbeam and oriented nanofibers. *ACS Appl. Mater. Inter.* **16**, 45861–45870 (2024).
30. Gao, H. et al. Bioinspired two-in-one nanotransistor sensor for the simultaneous measurements of electrical and mechanical cellular responses. *Sci. Adv.* **8**, eabn2485
31. Cohen, A. et al. Mechanism and reversal of drug-induced nephrotoxicity on a chip. *Sci. Transl. Med.* **13**, eabd6299 (2021).
32. Choi, M.-S. et al. Enhanced electrophysiological activity and neurotoxicity screening of environmental chemicals using 3D neurons from human neural precursor cells purified with PSA-NCAM. *Ecotoxicol. Environ. Saf.* **280**, 116516 (2024).
33. Wang, Y. et al. 3D-bioprinted hepar-on-a-chip implanted in graphene-based plasmonic sensors. *ACS Sens* **9**, 3423–3432 (2024).
34. Zhou, Q. et al. Liver injury-on-a-chip: microfluidic co-cultures with integrated biosensors for monitoring liver cell signaling during injury. *Lab Chip* **15**, 4467–4478 (2015).
35. Gao, F. et al. Multi-site dynamic recording for Aβ oligomers-induced Alzheimer's disease in vitro based on neuronal network chip. *Biosens. Bioelectron.* **133**, 183–191 (2019).
36. Kim, M. et al. Multimodal characterization of cardiac organoids using integrations of pressure-sensitive transistor arrays with three-dimensional liquid metal electrodes. *Nano Lett.* **22**, 7892–7901 (2022).
37. Gao, H. et al. Graphene-integrated mesh electronics with converged multifunctionality for tracking multimodal excitation-contraction dynamics in cardiac microtissues. *Nat. Comm.* **15**, 2321 (2024).
38. Dou, W. et al. A carbon-based biosensing platform for simultaneously measuring the contraction and electrophysiology of iPSC-cardiomyocyte monolayers. *ACS Nano* **16**, 11278–11290 (2022).
39. Fang, J. et al. Cardiomyocyte electrical-mechanical synchronized model for high-content, dose-quantitative and time-dependent drug assessment. *Microsyst. Nanoeng.* **7**, 26 (2021).
40. Qian, F. et al. Simultaneous electrical recording of cardiac electrophysiology and contraction on chip. *Lab Chip* **17**, 1732–1739 (2017).
41. Kim, J. et al. Development of albumin monitoring system with hepatic hypoxia-on-a-chip. *Talanta* **260**, 124592 (2023).
42. Zhang, B. -y. et al. A pH-sensitive fluorescent probe based on hemicyanine dyes for responding microenvironment changes of cardiomyocytes induced by Zn2+. *Microchem. J.* **193**, 109085 (2023).
43. Han, H. et al. Cardiomyocyte-based multimodal biosensing platform for dynamic functional assessment of bioinspired engineered respiratory virus-induced myocarditis. *ACS Nano* **19**, 28502–28515 (2025).
44. Yan, L. P. et al. Soft electrodes for electrochemical and electrophysiological monitoring of beating cardiomyocytes. *Angew. Chem. Int. Ed.* **61**, e202203757 (2022).
45. Schneider, O. et al. Fusing spheroids to aligned μ-tissues in a heart-on-chip featuring oxygen sensing and electrical pacing capabilities. *Mater. Today Bio.* **15**, 100280 (2022).
46. Liu, Y. et al. Microchip-based ELISA strategy for the detection of low-level disease biomarker in serum. *Anal. Chim. Acta* **650**, 77–82 (2009).
47. Sun, S., Yang, M., Kostov, Y. & Rasooly, A. ELISA-LOC: lab-on-a-chip for enzyme-linked immunodetection. *Lab Chip* **10**, 2093–2100 (2010).
48. Osaki, T., Uzel, S. G. M. & Kamm, R. D. Microphysiological 3D model of amyotrophic lateral sclerosis (ALS) from human iPS-derived muscle cells and optogenetic motor neurons. *Sci. Adv.* **4**, eaat5847
49. Xu, R. N., Fan, L., Rieser, M. J. & El-Shourbagy, T. A. Recent advances in high-throughput quantitative bioanalysis by LC–MS/MS. *J. Pharm. Biomed. Anal.* **44**, 342–355 (2007).
50. Spijkers, X. M. et al. A directional 3D neurite outgrowth model for studying motor axon biology and disease. *Sci. Rep.* **11**, 2080 (2021).
51. Freag, M. S. et al. Human nonalcoholic steatohepatitis on a chip. *Hepatol. Commun.* **5**, 217–233 (2021).
52. Wang, Y., Wang, L., Guo, Y., Zhu, Y. & Qin, J. Engineering stem cell-derived 3D brain organoids in a perfusable organ-on-a-chip system. *RSC Adv.* **8**, 1677–1685 (2018).
53. Maoz, B. M. et al. A linked organ-on-chip model of the human neurovascular unit reveals the metabolic coupling of endothelial and neuronal cells. *Nat. Biotechnol.* **36**, 865–874 (2018).
54. Chaubey, A. & Malhotra, B. D. Mediated biosensors. *Biosens. Bioelectron.* **17**, 441–456 (2002).
55. Grieshaber, D., MacKenzie, R., Vörös, J. & Reimhult, E. Electrochemical biosensors-sensor principles and architectures. *Sensors* **8**, 1400–1458 (2008).
56. Ortega, M. A. et al. Muscle-on-a-chip with an on-site multiplexed biosensing system for in situ monitoring of secreted IL-6 and TNF-α. *Lab Chip* **19**, 2568–2580 (2019).
57. Jin, Z. H., Liu, Y. L., Fan, W. T. & Huang, W. H. Integrating flexible electrochemical sensor into microfluidic chip for simulating and monitoring vascular mechanotransduction. *Small* **16**, e1903204 (2020).
58. Liu, Y., Liu, Y., Matharu, Z., Rahimian, A. & Revzin, A. Detecting multiple cell-secreted cytokines from the same aptamer-functionalized electrode. *Biosens. Bioelectron.* **64**, 43–50 (2015).

59. Liu, Y., Tuleouva, N., Ramanculov, E. & Revzin, A. Aptamer-based electrochemical biosensor for interferon gamma detection. *Anal. Chem.* **82**, 8131–8136 (2010).
60. Lorenz, W. & Schulze, K. D. Zur Anwendung der Transformations—Impedanzspektrometrie. *J. Electroanal. Chem. Interfacial Electrochem.* **65**, 141–153 (1975).
61. Shin, S. R. et al. Label-free and regenerative electrochemical microfluidic biosensors for continual monitoring of cell secretomes. *Adv. Sci.* **4**, 1600522 (2017).
62. Mou, L., Xia, Y. & Jiang, X. Epidermal sensor for potentiometric analysis of metabolite and electrolyte. *Anal. Chem.* **93**, 11525–11531 (2021).
63. Mou, L., Xia, Y. & Jiang, X. Liquid metal-polymer conductor-based wireless, battery-free epidermal patch. *Biosens. Bioelectron.* **197**, 113765 (2022).
64. Park, J., Meissner, R., Ducloux, O., Renaud, P. & Fujita, H. A calcium ion-selective electrode array for monitoring the activity of HepG2/C3As in a microchannel. *Sens. Actuators B. Chem.* **174**, 473–477 (2012).
65. Mir, M., Palma-Florez, S., Lagunas, A., López-Martínez, M. J. & Samitier, J. Biosensors integration in blood–brain barrier-on-a-chip: emerging platform for monitoring neurodegenerative diseases. *ACS Sens* **7**, 1237–1247 (2022).
66. Ellis, B. W. et al. Human Heart Anoxia and Reperfusion Tissue (HEART) model for the rapid study of exosome bound miRNA expression as biomarkers for myocardial infarction. *Small* **18**, e2201330 (2022).
67. Wang, Q. et al. Research advances on surface plasmon resonance biosensors. *Nanoscale* **14**, 564–591 (2022).
68. Pitarke, J. M., Silkin, V. M., Chulkov, E. V. & Echenique, P. M. Theory of surface plasmons and surface-plasmon polaritons. *Rep. Prog. Phys.* **70**, 1 (2007).
69. Ruppin, R. Surface polaritons of a left-handed medium. *Phys. Lett. A* **277**, 61–64 (2000).
70. Wei, X. et al. An enzyme-free surface plasmon resonance imaging biosensing method for highly sensitive detection of microRNA based on catalytic hairpin assembly and spherical nucleic acid. *Anal. Chim. Acta* **1108**, 21–27 (2020).
71. Huang, C. J., Lin, Z. E., Yang, Y. S., Chan, H. W. & Chen, W. Y. Neutralized chimeric DNA probe for detection of single nucleotide polymorphism on surface plasmon resonance biosensor. *Biosens. Bioelectron.* **99**, 170–175 (2018).
72. Yang, J.-W. et al. Liver-on-a-chip integrated with label-free optical biosensors for rapid and continuous monitoring of drug-induced toxicity. *Small* **20**, 2403560 (2024).
73. Ortega, M. A. et al. In Situ LSPR Sensing of Secreted Insulin in Organ-on-Chip. *Biosensors* **11** https://doi.org/10.3390/bios11050138 (2021).
74. Wu, S.-H., Lee, K.-L., Chiou, A., Cheng, X. & Wei, P.-K. Optofluidic platform for real-time monitoring of live cell secretory activities using fano resonance in gold nanoslits. *Small* **9**, 3532–3540 (2013).
75. Cognetti, J. S. et al. A photonic biosensor-integrated tissue chip platform for real-time sensing of lung epithelial inflammatory markers. *Lab Chip* **23**, 239–250 (2023).
76. Chen, Y. et al. A biochemical sensor with continuous extended stability in vivo. *Nat. Biomed. Eng.* **9**, 1517–1530 (2025).
77. Zargartalebi, H. et al. Active-reset protein sensors enable continuous in vivo monitoring of inflammation. *Science* **386**, 1146–1153 (2024).
78. Saateh, A. et al. Long-term and continuous plasmonic oligonucleotide monitoring enabled by regeneration approach. *Angew. Chem. Int. Ed.* **63**, e202410076 (2024).
79. Vargas, E. et al. Using cell membranes as recognition layers to construct ultrasensitive and selective bioelectronic affinity sensors. *J. Am. Chem. Soc.* **144**, 17700–17708 (2022).
80. Qing, R. et al. Scalable biomimetic sensing system with membrane receptor dual-monolayer probe and graphene transistor arrays. *Sci. Adv.* **9**, eadf1402 (2023).
81. Ribeiro, A. J. S. et al. Contractility of single cardiomyocytes differentiated from pluripotent stem cells depends on physiological shape and substrate stiffness. *Proc. Natl. Acad. Sci. USA* **112**, 12705–12710 (2015).
82. Gehre, C. et al. Real time monitoring of oxygen uptake of hepatocytes in a microreactor using optical microsensors. *Sci. Rep.* **10**, 13700 (2020).
83. Herland, A. et al. Distinct contributions of astrocytes and pericytes to neuroinflammation identified in a 3D human blood-brain barrier on a chip. *PLoS One* **11**, e0150360 (2016).
84. Liu, S. et al. Biosensors integrated 3D organoid/organ-on-a-chip system: A real-time biomechanical, biophysical, and biochemical monitoring and characterization. *Biosens. Bioelectron.* **231**, 115285 (2023).
85. Peel, S. et al. Introducing an automated high content confocal imaging approach for Organs-on-Chips. *Lab Chip* **19**, 410–421 (2019).
86. Di, Z. et al. Ultra high content image analysis and phenotype profiling of 3D cultured micro-tissues. *PLoS One* **9**, e109688 (2014).
87. Joshi, P., Datar, A., Yu, K.-N., Kang, S.-Y. & Lee, M.-Y. High-content imaging assays on a miniaturized 3D cell culture platform. *Toxicol. Vitr.* **50**, 147–159 (2018).
88. Joshi, P., Kang, S.-Y., Yu, K.-N., Kothapalli, C. & Lee, M.-Y. High-content imaging of 3D-cultured neural stem cells on a 384-pillar plate for the assessment of cytotoxicity. *Toxicol. Vitr.* **65**, 104765 (2020).
89. MacQueen, L., Chebotarev, O., Simmons, C. A. & Sun, Y. Miniaturized platform with on-chip strain sensors for compression testing of arrayed materials. *Lab Chip* **12**, 4178–4184 (2012).
90. Kim, D.-S., Jeong, Y.-J., Lee, B.-K., Shanmugasundaram, A. & Lee, D.-W. Piezoresistive sensor-integrated PDMS cantilever: A new class of device for measuring the drug-induced changes in the mechanical activity of cardiomyocytes. *Sens. Actuators B. Chem.* **240**, 566–572 (2017).
91. Zhang, Y. et al. Strain sensor on a chip for quantifying the magnitudes of tensile stress on cells. *Microsyst. Nanoeng.* **10**, 88 (2024).
92. Lyu, Q. et al. A soft and ultrasensitive force sensing diaphragm for probing cardiac organoids instantaneously and wirelessly. *Nat. Commun.* **13**, 7259 (2022).
93. Wang, L. et al. Crack sensing of cardiomyocyte contractility with high sensitivity and stability. *ACS Nano* **16**, 12645–12655 (2022).
94. Virtanen, J., Toivanen, M., Toimela, T., Heinonen, T. & Tuukkanen, S. Direct measurement of contraction force in human cardiac tissue model using piezoelectric cantilever sensor technique. *Curr. Appl Phys.* **20**, 155–160 (2020).
95. Mannhardt, I., Warncke, C., Trieu, H. K., Müller, J. & Eschenhagen, T. Piezobending actuators for isometric or auxotonic contraction analysis of engineered heart tissue. *J. Tissue Eng. Regen. Med.* **13**, 3–11 (2019).
96. Nguyen, T. D. et al. Piezoelectric nanoribbons for monitoring cellular deformations. *Nat. Nanotechnol.* **7**, 587–593 (2012).
97. Adadi, N. et al. Electrospun fibrous PVDF-TrFe scaffolds for cardiac tissue engineering, differentiation, and maturation. *Adv. Mater. Technol.* **5**, 1900820 (2020).
98. Chen, H. et al. Drug-screening triboelectric nanogenerator-based strain sensor for cardiomyocyte contractility. *Nano Energy* **109**, 108251 (2023).
99. Zhang, T. et al. Flexible sensing platform based on negative pressure triboelectric nanogenerators and microelectrode array for long-term synchronous monitoring of electrophysiological and mechanical beating in cardiomyocytes. *ACS Sens.* https://doi.org/10.1021/acssensors.5c00753 (2025).
100. Araromi, O. A. et al. Optimization of thin-film highly-compliant elastomer sensors for contractility measurement of muscle cells. *Extrem. Mech. Lett.* **9**, 1–10 (2016).
101. Boschi, A. et al. Interferometric biosensor for high sensitive label-free recording of HiPS cardiomyocytes contraction in vitro. *Nano Lett.* **24**, 6451–6458 (2024).
102. Li, T. et al. Utilizing tissues self-assembled in fiber optic-based "Chinese Guzheng Strings" for contractility sensing and drug efficacy evaluation: a practical approach. *Small* **21**, 2406144 (2025).
103. Li, L. et al. Graphene hybrid anisotropic structural color film for cardiomyocytes' monitoring. *Adv. Funct. Mater.* **30**, 1906353 (2020).
104. Sun, L., Chen, Z., Xu, D. & Zhao, Y. Electroconductive and anisotropic structural color hydrogels for visual heart-on-a-chip construction. *Adv. Sci.* **9**, 2105777 (2022).
105. Xu, D. et al. Living anisotropic structural color hydrogels for cardiotoxicity screening. *ACS Nano* **17**, 15180–15188 (2023).
106. Chen, Z. et al. Cardiomyocytes-actuated morpho butterfly wings. *Adv. Mater.* **31**, 1805431 (2019).
107. Zhu, Y. et al. A biomimetic human lung-on-a-chip with colorful display of microphysiological breath. *Adv. Mater.* **34**, e2108972 (2022).
108. Shi, K. et al. Advanced passive 3D bioelectronics: powerful tool for the cardiac electrophysiology investigation. *Microsyst. Nanoeng.* **11**, 50 (2025).
109. Liu, H. et al. Heart-on-a-chip model with integrated extra- and intracellular bioelectronics for monitoring cardiac electrophysiology under acute hypoxia. *Nano Lett.* **20**, 2585–2593 (2020).
110. Xu, D., Mo, J., Xie, X. & Hu, N. In-cell nanoelectronics: opening the door to intracellular electrophysiology. *Nano-Micro Lett.* **13**, 127 (2021).
111. Kalmykov, A. et al. Organ-on-e-chip: Three-dimensional self-rolled biosensor array for electrical interrogations of human electrogenic spheroids. *Sci. Adv.* **5**, eaax0729 (2019).

112. Xue, M. et al. Composite additive manufacturing for suspended microelectrode arrays: Advancing oriented myocardial tissue culturing and electrophysiological sensing. *Biosens. Bioelectron.* **287**, 117686 (2025).
113. Wang, G. et al. An optogenetics- and imaging-assisted simultaneous multiple patch-clamp recording system for decoding complex neural circuits. *Nat. Protoc.* **10**, 397–412 (2015).
114. Fertig, N., Blick, R. H. & Behrends, J. C. Whole cell patch clamp recording performed on a planar glass chip. *Biophys. J.* **82**, 3056–3062 (2002).
115. Hai, A., Shappir, J. & Spira, M. E. In-cell recordings by extracellular microelectrodes. *Nat. Methods* **7**, 200–202 (2010).
116. Hu, N. et al. Intracellular recording of cardiomyocyte action potentials by nanobranched microelectrode array. *Biosens. Bioelectron.* **169**, 112588 (2020).
117. Xie, C., Lin, Z., Hanson, L., Cui, Y. & Cui, B. Intracellular recording of action potentials by nanopillar electroporation. *Nat. Nanotechnol.* **7**, 185–190 (2012).
118. Robinson, J. T. et al. Vertical nanowire electrode arrays as a scalable platform for intracellular interfacing to neuronal circuits. *Nat. Nanotechnol.* **7**, 180–184 (2012).
119. Abbott, J., Ye, T., Ham, D. & Park, H. Optimizing nanoelectrode arrays for scalable intracellular electrophysiology. *Acc. Chem. Res.* **51**, 600–608 (2018).
120. Duan, X. et al. Intracellular recordings of action potentials by an extracellular nanoscale field-effect transistor. *Nat. Nanotechnol.* **7**, 174–179 (2012).
121. Lin, Z. C., Xie, C., Osakada, Y., Cui, Y. & Cui, B. Iridium oxide nanotube electrodes for sensitive and prolonged intracellular measurement of action potentials. *Nat. Comm.* **5**, 3206 (2014).
122. Hai, A. & Spira, M. E. On-chip electroporation, membrane repair dynamics and transient in-cell recordings by arrays of gold mushroom-shaped microelectrodes. *Lab Chip* **12**, 2865–2873 (2012).
123. Gu, Y. et al. Three-dimensional transistor arrays for intra- and inter-cellular recording. *Nat. Nanotechnol.* **17**, 292–300 (2022).
124. Gross, G. W., Rieske, E., Kreutzberg, G. W. & Meyer, A. A new fixed-array multimicroelectrode system designed for long-term monitoring of extracellular single unit neuronal activity in vitro. *Neurosci. Lett.* **6**, 101–105 (1977).
125. Thomas, C. A., Springer, P. A., Loeb, G. E., Berwald-Netter, Y. & Okun, L. M. A miniature microelectrode array to monitor the bioelectric activity of cultured cells. *Exp. Cell Res.* **74**, 61–66 (1972).
126. Connolly, P., Clark, P., Curtis, A. S. G., Dow, J. A. T. & Wilkinson, C. D. W. An Extracellular microelectrode Array for monitoring electrogenic cells in culture. *Biosens. Bioelectron.* **5**, 223–234 (1990).
127. Cohen-Karni, T., Timko, B. P., Weiss, L. E. & Lieber, C. M. Flexible electrical recording from cells using nanowire transistor arrays. *Proc. Natl. Acad. Sci. USA* **106**, 7309–7313 (2009).
128. Spira, M. E. & Hai, A. Multi-electrode array technologies for neuroscience and cardiology. *Nat. Nanotechnol.* **8**, 83–94 (2013).
129. Selinger, J. V., Pancrazio, J. J. & Gross, G. W. Measuring synchronization in neuronal networks for biosensor applications. *Biosens. Bioelectron.* **19**, 675–683 (2004).
130. Erickson, J., Tooker, A., Tai, Y. C. & Pine, J. Caged neuron MEA: A system for long-term investigation of cultured neural network connectivity. *J. Neurosci. Methods* **175**, 1–16 (2008).
131. Liu, Y. et al. SWCNTs/PEDOT:PSS nanocomposites-modified microelectrode arrays for revealing locking relations between burst and local field potential in cultured cortical networks. *Biosens. Bioelectron.* **253**, 116168 (2024).
132. Xu, S. et al. High-Throughput PEDOT:PSS/PtNPs-modified microelectrode array for simultaneous recording and stimulation of hippocampal neuronal networks in gradual learning process. *ACS Appl. Mater. Inter.* **14**, 15736–15746 (2022).
133. Rabieh, N. et al. On-chip, multisite extracellular and intracellular recordings from primary cultured skeletal myotubes. *Sci. Rep.* **6**, 36498 (2016).
134. Holzreuter, M. A. & Segerink, L. I. Innovative electrode and chip designs for transendothelial electrical resistance measurements in organs-on-chips. *Lab Chip* **24**, 1121–1134 (2024).
135. Henry, O. Y. F. et al. Organs-on-chips with integrated electrodes for transepithelial electrical resistance (TEER) measurements of human epithelial barrier function. *Lab Chip* **17**, 2264–2271 (2017).
136. Srinivasan, B. et al. TEER measurement techniques for in vitro barrier model systems. *SLAS Technol.* **20**, 107–126 (2015).
137. Sei, Y. J., Ahn, S. I., Virtue, T., Kim, T. & Kim, Y. Detection of frequency-dependent endothelial response to oscillatory shear stress using a microfluidic transcellular monitor. *Sci. Rep.* **7**, 10019 (2017).
138. Ahn, S. I. et al. Microengineered human blood-brain barrier platform for understanding nanoparticle transport mechanisms. *Nat. Commun.* **11**, 175 (2020).
139. Ceccarelli, M. C. et al. Real-time monitoring of a 3D blood–brain barrier model maturation and integrity with a sensorized microfluidic device. *Lab Chip* **24**, 5085–5100 (2024).
140. Shaughnessey, E. M. et al. Evaluation of rapid transepithelial electrical resistance (TEER) measurement as a metric of kidney toxicity in a high-throughput microfluidic culture system. *Sci. Rep.* **12**, 13182 (2022).
141. Maoz, B. M. et al. Organs-on-Chips with combined multi-electrode array and transepithelial electrical resistance measurement capabilities. *Lab Chip* **17**, 2294–2302 (2017).
142. Farooqi, H. M. U. et al. Real-time monitoring of liver fibrosis through embedded sensors in a microphysiological system. *Nano Converg.* **8**, 3 (2021).
143. Brandauer, K. et al. Sensor-integrated gut-on-a-chip for monitoring senescence-mediated changes in the intestinal barrier. *Lab Chip* **25**, 1694–1706 (2025).
144. Schellberg, B. G., Koppes, A. N. & Koppes, R. A. In situ monitoring of barrier function on-chip via automated, non-invasive luminescence sensing. *Lab Chip* https://doi.org/10.1039/D4LC01090F (2025).
145. Lucchetti, M. et al. Integration of multiple flexible electrodes for real-time detection of barrier formation with spatial resolution in a gut-on-chip system. *Microsyst. Nanoeng.* **10**, 18 (2024).
146. Zhu, M. et al. Flexible Electrodes for In Vivo and In Vitro Electrophysiological Signal Recording. *Adv. Healthc. Mater.* **10**, 2100646 (2021).
147. Feiner, R. et al. Engineered hybrid cardiac patches with multifunctional electronics for online monitoring and regulation of tissue function. *Nat. Mater.* **15**, 679–685 (2016).
148. Jiang, Y. et al. Topological supramolecular network enabled high-conductivity, stretchable organic bioelectronics. *Science* **375**, 1411–1417 (2022).
149. Tsai, D., Sawyer, D., Bradd, A., Yuste, R. & Shepard, K. L. A very large-scale microelectrode array for cellular-resolution electrophysiology. *Nat. Comm.* **8**, 1802 (2017).
150. Jiang, N. et al. High-throughput electromechanical coupling chip systems for real-time 3D invasion/migration assay of cells. *Adv. Sci.* **10**, 2300882 (2023).
151. Jahnke, H.-G. et al. Electrochemical live monitoring of tumor cell migration out of micro-tumors on an innovative multiwell high-dense microelectrode array. *Sci. Rep.* **9**, 13875 (2019).
152. Hall, M. S. et al. Fibrous nonlinear elasticity enables positive mechanical feedback between cells and ECMs. *Proc. Natl. Acad. Sci. USA* **113**, 14043–14048 (2016).
153. Przybyla, L., Lakins, J. N., Sunyer, R., Trepat, X. & Weaver, V. M. Monitoring developmental force distributions in reconstituted embryonic epithelia. *Methods* **94**, 101–113 (2016).
154. Zareei, A. et al. A lab-on-chip ultrasonic platform for real-time and non-destructive assessment of extracellular matrix stiffness. *Lab Chip* **20**, 778–788 (2020).
155. Wang, L. et al. Gut-on-a-chip for exploring the transport mechanism of Hg(II). *Microsyst. Nanoeng.* **9**, 2 (2023).
156. McCain, M. L., Sheehy, S. P., Grosberg, A., Goss, J. A. & Parker, K. K. Recapitulating maladaptive, multiscale remodeling of failing myocardium on a chip. *Proc. Natl. Acad. Sci.* **110**, 9770–9775 (2013).
157. She, W. et al. Hydrogel strain sensors for integrating into dynamic organ-on-a-chip. *Small* **21**, 2407704 (2025).
158. Bai, H. et al. Mechanical control of innate immune responses against viral infection revealed in a human lung alveolus chip. *Nat. Comm.* **13**, 1928 (2022).
159. Zheng, W. et al. A microfluidic flow-stretch chip for investigating blood vessel biomechanics. *Lab Chip* **12**, 3441–3450 (2012).
160. Wang, J., Heo, J. & Hua, S. Z. Spatially resolved shear distribution in microfluidic chip for studying force transduction mechanisms in cells. *Lab Chip* **10**, 235–239 (2010).
161. Zhou, M. et al. Development of a functional glomerulus at the organ level on a chip to mimic hypertensive nephropathy. *Sci. Rep.* **6**, 31771 (2016).
162. Velasco, V., Soucy, P., Keynton, R. & Williams, S. J. A microfluidic impedance platform for real-time, in vitro characterization of endothelial cells undergoing fluid shear stress. *Lab Chip* **22**, 4705–4716 (2022).
163. Liu, M.-C. et al. Electrofluidic pressure sensor embedded microfluidic device: a study of endothelial cells under hydrostatic pressure and shear stress combinations. *Lab Chip* **13**, 1743–1753 (2013).

164. Rivera, K. R. et al. Integrated phosphorescence-based photonic biosensor (iPOB) for monitoring oxygen levels in 3D cell culture systems. *Biosens. Bioelectron.* **123**, 131–140 (2019).
165. Khalid, M. A. U. et al. High performance inkjet printed embedded electrochemical sensors for monitoring hypoxia in a gut bilayer microfluidic chip. *Lab Chip* **22**, 1764–1778 (2022).
166. Shellman, Y. G. et al. Fast response temperature measurement and highly reproducible heating methods for 96-well plates. *Biotechniques* **36**, 968–976 (2004).
167. Reichen, M., Veraitch, F. S. & Szita, N. Development of a multiplexed microfluidic platform for the automated cultivation of embryonic stem cells. *SLAS Technol.* **18**, 519–529 (2013).
168. Gillot, F. et al. On-chip thermal calibration with 8 CB liquid crystal of microthermal device. *Lab Chip* **7**, 1600–1602 (2007).
169. Qiao, J., Mu, X. & Qi, L. Construction of fluorescent polymeric nanothermometers for intracellular temperature imaging: A review. *Biosens. Bioelectron.* **85**, 403–413 (2016).
170. Larina, I. V., Larin, K. V. & Esenaliev, R. O. Real-time optoacoustic monitoring of temperature in tissues. *J. Phys. D Appl. Phys.* **38**, 2633 (2005).
171. da Ponte, R. M. et al. Monolithic integration of a smart temperature sensor on a modular silicon-based organ-on-a-chip device. *Sens. Actuator Phys.* **317**, 112439 (2021).
172. Yang, Z. et al. Carbonized silk nanofibers in biodegradable, flexible temperature sensors for extracellular environments. *ACS Appl. Mater. Inter.* **14**, 18110–18119 (2022).
173. Zhang, X. et al. Spatiotemporal cell control via high-precision electronic regulation of microenvironmental pH. *Nano Lett.* **24**, 15645–15651 (2024).
174. Aydogmus, H. et al. An organ-on-chip device with integrated charge sensors and recording microelectrodes. *Sci. Rep.* **13**, 8062 (2023).
175. Yang, L. et al. A 640 × 640 ISFET array for detecting cell metabolism. *J. Semiconductors* **44**, 024101 (2023).
176. Luo, Y., Song, Y., Wang, J., Xu, T. & Zhang, X. Integrated mini-pillar platform for wireless real-time cell monitoring. *Research* **7**, 0422.
177. Park, J. S. et al. Intracellular cardiomyocytes potential recording by planar electrode array and fibroblasts co-culturing on multi-modal CMOS chip. *Biosens. Bioelectron.* **144**, 111626 (2019).
178. Fuchs, S. et al. In-line analysis of organ-on-chip systems with sensors: integration, fabrication, challenges, and potential. *ACS Biomater. Sci. Eng.* **7**, 2926–2948 (2021).
179. Xu, F. et al. Architecture design and advanced manufacturing of heart-on-a-chip: scaffolds, stimulation and sensors. *Microsyst. Nanoeng.* **10**, 96 (2024).
180. Giovangrandi, L., Gilchrist, K. H., Whittington, R. H. & T.A. Kovacs, G. Low-cost microelectrode array with integrated heater for extracellular recording of cardiomyocyte cultures using commercial flexible printed circuit technology. *Sens. Actuators B. Chem.* **113**, 545–554 (2006).
181. Lopez, C. M. et al. A Multimodal CMOS MEA for high-throughput intracellular action potential measurements and impedance spectroscopy in drug-screening applications. *IEEE J. Solid-State Circuits* **53**, 3076–3086 (2018).
182. Liu, Y. et al. Neuromodulatory compensation of cortical neural activity on electrodeposited Pt/Ir modified microelectrode arrays for temperature transients. *ACS Appl. Mater. Inter.* **16**, 44538–44548 (2024).
183. Zhang, W. et al. Flexible beam-based microelectrode arrays integrated with oriented nanofiber scaffolds for electrophysiological monitoring of cardiac tissue. *Acta Biomater.* https://doi.org/10.1016/j.actbio.2025.06.005 (2025).
184. Park, Y. et al. Three-dimensional, multifunctional neural interfaces for cortical spheroids and engineered assembloids. *Sci. Adv.* **7**, eabf9153.
185. Kim, K. et al. Highly stretchable 3D microelectrode array for noninvasive functional evaluation of cardiac spheroids and midbrain organoids. *Adv. Mater.* **37**, 2412953 (2025).
186. Hu, L. et al. Hydrogel-Based Flexible Electronics. *Adv. Mater.* **35**, 2205326 (2023).
187. Martinelli, E. et al. The e-Flower: A hydrogel-actuated 3D MEA for brain spheroid electrophysiology. *Sci. Adv.* **10**, eadp8054 (2024).
188. Le Floch, P. et al. Stretchable mesh nanoelectronics for 3D single-cell chronic electrophysiology from developing brain organoids. *Adv. Mater.* **34**, 2106829 (2022).
189. Shin, S. R. et al. Aptamer-based microfluidic electrochemical biosensor for monitoring cell-secreted trace cardiac biomarkers. *Anal. Chem.* **88**, 10019–10027 (2016).
190. la Cour, J. B., Generelli, S., Barbe, L. & Guenat, O. T. Low-cost disposable ALT electrochemical microsensors for in-vitro hepatotoxic assessment. *Sens. Actuators B. Chem.* **228**, 360–365 (2016).
191. Weltin, A. et al. Accessing 3D microtissue metabolism: lactate and oxygen monitoring in hepatocyte spheroids. *Biosens. Bioelectron.* **87**, 941–948 (2017).
192. Zhang, W. et al. Flexible microelectrode arrays based on vacuum filling for electrophysiology sensing of cardiomyocytes. *ACS Appl. Electron. Mater.* **6**, 6431–6439 (2024).
193. Sun, H. et al. Enhancing cardiomyocytes contraction force measuring in drug testing: Integration of a highly sensitive single-crystal silicon strain sensor into SU-8 cantilevers. *Biosens. Bioelectron.* **243**, 115756 (2024).
194. Christensen, R. K., von Halling Laier, C., Kiziltay, A., Wilson, S. & Larsen, N. B. 3D Printed Hydrogel Multiassay Platforms for Robust Generation of Engineered Contractile Tissues. *Biomacromolecules* **21**, 356–365 (2020).
195. Wu, S.-D., Weller, H., Vossmeyer, T. & Hsu, S. -h Motion Sensing by a Highly Sensitive Nanogold Strain Sensor in a Biomimetic 3D Environment. *ACS Appl. Mater. Inter.* **16**, 56599–56610 (2024).
196. Li, L. et al. Enhancing cardiomyocyte maturation via mechanical stimulation of 3d printed cardiac tissue using a origami-based 3D sensor and magnetic fields. *IEEE Int. Conf. on Nano/Mol. Med. Eng., NANOMED*, 83-86 (2024).
197. Zhao, R., Boudou, T., Wang, W.-G., Chen, C. S. & Reich, D. H. Decoupling cell and matrix mechanics in engineered microtissues using magnetically actuated microcantilevers. *Adv. Mater.* **25**, 1699–1705 (2013).
198. Michelini, E. et al. Smartphone-based multicolor bioluminescent 3D spheroid biosensors for monitoring inflammatory activity. *Biosens. Bioelectron.* **123**, 269–277 (2019).
199. Sheyn, D. et al. Bone-chip system to monitor osteogenic differentiation using optical imaging. *Microfluid. Nanofluid.* **23**, 99 (2019).
200. Araujo-Gomes, N. et al. Bioluminescence imaging on-chip platforms for non-invasive high-content bioimaging. *Biosens. Bioelectron.* **237**, 115510 (2023).
201. Rennert, K. et al. A microfluidically perfused three dimensional human liver model. *Biomaterials* **71**, 119–131 (2015).
202. Jalili-Firoozinezhad, S. et al. A complex human gut microbiome cultured in an anaerobic intestine-on-a-chip. *Nat. Biomed. Eng.* **3**, 520–531 (2019).
203. Li, J. et al. 3D printed neural tissues with in situ optical dopamine sensors. *Biosens. Bioelectron.* **222**, 114942 (2023).
204. Asif, A., Kim, K. H., Jabbar, F., Kim, S. & Choi, K. H. Real-time sensors for live monitoring of disease and drug analysis in microfluidic model of proximal tubule. *Microfluid. Nanofluid.* **24**, 43 (2020).
205. Farooqi, H. M. U., Khalid, M. A. U., Kim, K. H., Lee, S. R. & Choi, K. H. Real-time physiological sensor-based liver-on-chip device for monitoring drug toxicity. *J. Micromech. Microeng.* **30**, 115013 (2020).
206. Khalid, M. A. U. et al. A lung cancer-on-chip platform with integrated biosensors for physiological monitoring and toxicity assessment. *Biochem. Eng. J.* **155**, 107469 (2020).
207. Grant, J. et al. Establishment of physiologically relevant oxygen gradients in microfluidic organ chips. *Lab Chip* **22**, 1584–1593 (2022).
208. Zirath, H. et al. Bridging the academic-industrial gap: application of an oxygen and pH sensor-integrated lab-on-a-chip in nanotoxicology. *Lab Chip* **21**, 4237–4248 (2021).
209. Shahabipour, F. et al. Engineering organ-on-a-chip systems to model viral infections. *Biofabrication* **15**, 022001 (2023).
210. Zhang, M. et al. Biomimetic human disease model of SARS-CoV-2-induced lung injury and immune responses on organ chip system. *Adv. Sci.* **8**, 2002928 (2021).
211. Ortega-Prieto, A. M. et al. 3D microfluidic liver cultures as a physiological preclinical tool for hepatitis B virus infection. *Nat. Comm.* **9**, 682 (2018).
212. Pelkonen, A. et al. A modular brain-on-a-chip for modelling epileptic seizures with functionally connected human neuronal networks. *Biosens. Bioelectron.* **168**, 112553 (2020).
213. Gijzen, L. et al. An intestine-on-a-chip model of plug-and-play modularity to study inflammatory processes. *SLAS Technol.* **25**, 585–597 (2020).
214. Li, Y., Xu, M., Zhu, Z., Xu, F. & Chen, B. Transendothelial electrical resistance measurement by a microfluidic device for functional study of endothelial barriers in inflammatory bowel disease. *Front. Bioeng. Biotechnol.* **11**, 1236610 (2023).
215. Zhang, T. X. et al. Research on vascular thrombosis detection methods based on fiber bragg grating sensing. *IEEE Sens. J.* **25**, 489–497 (2025).
216. Schlunder, K. et al. Microphysiological pancreas-on-chip platform with integrated sensors to model endocrine function and metabolism. *Lab Chip* **24**, 2080–2093 (2024).

217. Glieberman, A. L. et al. Synchronized stimulation and continuous insulin sensing in a microfluidic human Islet on a Chip designed for scalable manufacturing. *Lab Chip* **19**, 2993–3010 (2019).
218. Rothbauer, M. et al. Integration of glucose and lactate biosensors into human cartilage-on-a-chip models for long-term monitoring of metabolic shifts in osteoarthritis. *Sens. Actuators B. Chem.* **427**, 137123 (2025).
219. Rothbauer, M. et al. Monitoring tissue-level remodelling during inflammatory arthritis using a three-dimensional synovium-on-a-chip with non-invasive light scattering biosensing. *Lab Chip* **20**, 1461–1471 (2020).
220. Foster, A. J. et al. Integrated in vitro models for hepatic safety and metabolism: evaluation of a human Liver-Chip and liver spheroid. *Arch. Toxicol.* **93**, 1021–1037 (2019).
221. Mastikhina, O. et al. Human cardiac fibrosis-on-a-chip model recapitulates disease hallmarks and can serve as a platform for drug testing. *Biomaterials* **233**, 119741 (2020).
222. Lee, J. et al. A heart-breast cancer-on-a-chip platform for disease modeling and monitoring of cardiotoxicity induced by cancer chemotherapy. *Small* **17**, 2004258 (2021).
223. Fan, W.-T., Zhao, Y., Hong, F., Liu, Y.-L. & Huang, W.-H. Vasculature-on-a-chip with stretchable sensor for recapitulating hemodynamics and electrochemical monitoring of endothelium. *Sci. China Chem.* **66**, 3314–3322 (2023).
224. Bi, C.-X. et al. Nanofiber-based stretchable electrodes for oriented culture and mechanotransduction monitoring of smooth muscle cells. *ACS Sens* **8**, 3248–3256 (2023).
225. Liu, N.-C., Liang, C.-C., Li, Y.-C. E. & Lee, I. C. A Real-time sensing system for monitoring neural network degeneration in an alzheimer's disease-on-a-chip model. *Pharmaceutics* **14** https://doi.org/10.3390/pharmaceutics14051022 (2022).
226. Hammack, A., Rihani, R. T., Black, B. J., Pancrazio, J. J. & Gnade, B. E. A patterned polystyrene-based microelectrode array for in vitro neuronal recordings. *Biomed. Microdevices* **20**, 48 (2018).